AFRL-RV-PS-
TR-2018-0074

ADAPTIVE SEISMIC DENOISING BASED ON THE SYNCHROSQUEEZED-CONTINUOUS WAVELET TRANSFORM AND BLOCK-THRESHOLDING

Charles A. Langston

Center for Earthquake Research and Information
University of Memphis
3876 Central Ave., Ste. 1
Memphis, TN 38152

01 March 2018

Final Report

AIR FORCE RESEARCH LABORATORY
Space Vehicles Directorate
3550 Aberdeen Ave SE
AIR FORCE MATERIEL COMMAND
KIRTLAND AIR FORCE BASE, NM 87117-5776

DTIC COPY

NOTICE AND SIGNATURE PAGE

AFRL-RV-PS-TR-2018-0074 HAS BEEN REVIEWED AND IS APPROVED FOR PUBLICATION IN ACCORDANCE WITH ASSIGNED DISTRIBUTION STATEMENT.

//SIGNED//	//SIGNED//
Dr. Frederick Schult	Dr. Thomas R. Caudill, Chief
Program Manager/AFRL/RVBYE	AFRL Battlespace Environment Division

REPORT DOCUMENTATION PAGE

Form Approved
OMB No. 0704-0188

1. REPORT DATE *(DD-MM-YYYY)*	**2. REPORT TYPE**	**3. DATES COVERED** *(From - To)*
01-03-2018	Final Report	01 Mar 2016 – 28 Feb 2018

4. TITLE AND SUBTITLE
Adaptive Seismic Denoising Based on the Synchrosqueezed-Continuous Wavelet Transform and Block-Thresholding

5a. CONTRACT NUMBER
FA9453-16-C-0015

5b. GRANT NUMBER

5c. PROGRAM ELEMENT NUMBER
62601F

6. AUTHOR(S)
Charles A. Langston

5d. PROJECT NUMBER
1010

5e. TASK NUMBER
PPM00019641

5f. WORK UNIT NUMBER
EF128703

7. PERFORMING ORGANIZATION NAME(S) AND ADDRESS(ES)
Center for Earthquake Research and Information
University of Memphis
3876 Central Ave., Ste. 1
Memphis, TN 38152

8. PERFORMING ORGANIZATION REPORT NUMBER

9. SPONSORING / MONITORING AGENCY NAME(S) AND ADDRESS(ES)
Air Force Research Laboratory
Space Vehicles Directorate
3550 Aberdeen Avenue SE
Kirtland AFB, NM 87117-5776

10. SPONSOR/MONITOR'S ACRONYM(S)
AFRL/RVBYE

11. SPONSOR/MONITOR'S REPORT NUMBER(S)
AFRL-RV-PS-TR-2018-0074

12. DISTRIBUTION / AVAILABILITY STATEMENT

Approved for public release; distribution is unlimited. (AFMC-2018-0396 dtd 18 Sep 2018)

13. SUPPLEMENTARY NOTES

14. ABSTRACT

The Continuous Wavelet Transform (CWT), short time window Fourier transform (STFT), and synchrosqueezed transform CWT (SS-CWT) have been applied to single channel seismic data to remove noise from signal and signal from noise. Several theoretical investigations culminated in 4 publications concerning Time-Frequency Representations (TFR) of seismic data and resulted in experimental software that was delivered to interested scientists at AFTAC. In addition, a MatLab software Graphical User Interface and associated inline function, "BCseis" (for Block Choice Seismic Analysis) has been written for experimental and routine processing of seismic data using hard and soft block thresholding, band-pass filtering, and seismogram decomposition by manipulating a time series' CWT. Studies of seismic data were performed for 2 SPE explosions recorded at Mina, NV, at the NVAR array, 12 AFTAC explosions recorded by the IRIS Community Wavefields experiment in northern Oklahoma, and a suspected small nuclear event in North Korea. Use of thresholding techniques significantly improved signal-to-noise ratios for events that can be buried by noise. However, array beamforming ability can be compromised if the resulting signal becomes uncorrelated over the aperture of the array.

15. SUBJECT TERMS
Signal Analysis, Filtering, Time-Frequency Representations, Noise Removal, Continuous Wavelet Transform, Synchrosqueezing

16. SECURITY CLASSIFICATION OF:			**17. LIMITATION OF ABSTRACT**	**18. NUMBER OF PAGES**	**19a. NAME OF RESPONSIBLE PERSON**
a. REPORT	**b. ABSTRACT**	**c. THIS PAGE**			Dr. Frederick Schult
Unclassified	Unclassified	Unclassified	Unlimited	44	**19b. TELEPHONE NUMBER** *(include area code)* (505) 846-6101

Standard Form 298 (Rev. 8-98)
Prescribed by ANSI Std. 239.18

This page is intentionally left blank.

Table of Contents

List of Figures and Tables

List of Figures

List of Tables

This page is intentionally left blank.

1. SUMMARY

The Continuous Wavelet Transform (CWT), short time window Fourier transform (STFT), and synchrosqueezed transform CWT (SS-CWT) have been applied to single channel seismic data to remove noise from signal and signal from noise. The common factor in these techniques is the manipulation of transform coefficients on the time-frequency or time-scale plane to find regions of signal that are significantly above inferred noise. Several theoretical investigations culminated in 4 publications concerning Time-Frequency Representations (TFR) of seismic data and resulted in experimental software that was delivered to interested scientists at AFTAC. In addition, a MatLab software Graphical User Interface (GUI) and associated inline function, "BCseis" (for Block Choice Seismic Analysis) has been written for experimental and routine processing of seismic data using hard and soft block thresholding, band-pass filtering, and seismogram decomposition by manipulating a time series' CWT.

Dramatic signal-to-noise ratio (SNR) improvements were obtained by using these methods on a variety of common seismological data sets including high-frequency microseisms, ocean bottom seismic data, and short-period and broadband earthquake and explosion data. These methods were also applied to phased array data to detect and analyze Source Physics Experiment (SPE) explosions at Mina, Nevada, at the NVAR CTBTO array station. Although signal-to-noise ratios could be dramatically improved using block thresholding techniques for the 905 Kg SPE-3 explosion, a surprising result was that the degree of noise removal using hard or soft thresholding methods adversely affected the ability of the array to form an adequate beam. Indeed, processing to form the highest SNR data essentially removed that part of the signal that was correlated over the array making a case for deployment of dense, high frequency arrays to improve beam performance. There was only marginal detection of the small, 88 Kg SPE-1 shot at NVAR.

A high-quality array data set became available in early 2017 from the Incorporated Research Institutions in Seismology (IRIS) Community Wavefields Seismic Experiment in northcentral Oklahoma. Dense arrays of 5Hz three-component seismometers and a broadband regional array recorded a variety of local and regional earthquakes. AFRL also performed a seismic experiment in July 2016 consisting of 12 explosions, 2000 – 250 lbs in size, at 3 distances (15, 35, 67 km) from the center of the experiment. Use of block thresholding techniques on the explosion data set dramatically improved signal-to-noise ratios and also the beam forming ability of the high frequency array. An analysis of TFRs of the time series also demonstrated a variety of noise sources in the area that served to mask the smaller, larger distance explosions.

Block thresholding was successfully applied to detecting a small inferred nuclear test in North Korea (May 12, 2010) using local data recorded by a broadband experiment in China.

2. INTRODUCTION

Seismic data are often corrupted by noise during the acquisition process. Seismic denoising aims at increasing the signal-to-noise ratio (SNR) by eliminating this additive noise through various signal processing steps, while preserving important features of the seismic signal. Spectral filtering, as a common approach for improving the SNR, is not effective for suppressing noise that has the same frequency content as the signal. Moreover, it can distort the signal (Douglas 1997) and/or generate artifacts prior to impulsive arrivals (Scherbaum 2001). Certainly, the problems of noise are quite large in the analysis of small signals from local and regional seismic events where detection, location, and discrimination are critical processes for seismic verification studies.

More effective noise suppression can be achieved through thresholding methods in time-frequency domains; such as using the S-transform (Pinnegar and Eaton, 2003; Schimmel and Gallart, 2007; Parolai 2009; Ditommaso et al., 2010, 2012; Tselentis et al., 2012), randon transform (Sabbione et al., 2013, 2015; Zhang et al., 2015), the wave packet transform (Galiana-Merino et al, 2003; Shuchong and Xun, 2014), f-x or f-k filtering (Bekara and van der Baan, 2009; Naghizadeh 2011; Naghizadeh and Sacchi, 2012; Chen and Ma, 2014), singular spectrum analysis (Oropeza and Sacchi, 2011), sparse transform based denoising (Chen et al., 2016), a mathematical morphology based denoising approach (Li et al., 2016), reduced-rank filtering (Velis et al., 2015), damped multichannel singular spectrum analysis (Huang et al., 2016), the non-local means (NLM) algorithm (Bonar and Sacchi 2012) or the continuous wavelet transform (Pazos et al., 2003; Sobolev and Lyubushin, 2006; Mousavi and Langston, 2016a, 2016c).

Bekara and van der Baan, (2009), Han and Van Der Baan, (2015), Gomez and Velis (2016) showed that seismic noise can be removed effectively using empirical mode decomposition (EMD). EMD (Huang et al. 1998) is a data driven time-frequency analysis technique that adaptively decomposes a signal into a set of localized, modulated oscillations termed intrinsic mode functions (IMFs).

Recently, a new reassignment technique termed synchrosqueezing (SS) was introduced as a powerful alternative to EMD (Daubechies et al 2011). SS produces a sharpened time-frequency representation (TFR) of the signal that highly localizes modulated oscillations. It has better mathematical support and adaptability properties compared to EMD (Thakur et al. 2013; Herrera et al. 2014; Herrera et al. 2015).

Meignen et al. (2012) and Ahrabian and Mandic (2015) have introduced denoising techniques based on synchrosqueezing for univariate and multivariate signals, respectively. These methods are based on identifying common modulated oscillations in elements of data. They outperformed wavelet and EMD based methods. Mousavi et al., (2016a) showed that a simple normalization step in the synchrosqueezed domain can improve the SNR of microseismic events.

Here we introduce several adaptive algorithms for automatic noise or signal removal based on the synchrosqueezed-continuous wavelet transform (SS-CWT), incorporating higher-

order statistics (HOS), general cross validation (GCV), and wavelet hard- and soft-thresholding for seismic data. Some methods take advantage of the mode decomposition property of the SS-CWT. Major components present in recorded data are thresholded separately based on data characteristics. Synthetic and real simulations show that the proposed method is effective for accurate denoising and increasing the SNR of microseismic and OBS data, as well as filtering out the seismic signal in the case of noise studies.

3. METHODS, ASSUMPTIONS, AND PROCEDURES

3.1. Theoretical Background

3.1.1. The CWT and Block Thresholding

The Fourier transform is a staple in seismology because of its relation to theory of linear systems and use in solving theoretical problems in wave propagation. Fourier transformation of a time domain signal into the frequency domain allows integral operations in time, such as convolution or correlation, to become simple algebraic operations. But because the Fourier basis functions are infinitely long sinusoids for the Fourier transform, or periodic sinusoids for the discrete Fourier transform, signal information at particular times spreads over the entire frequency band.

The continuous wavelet transform, on the other hand, is a transform with two independent variables, scale *a*, and time lag τ, that produces a map of amplitude at scale vs time lag for the signal. The Morlet-Grossmann definition (Grossmann et al. 1989; Starck et al. 2010) for the CWT is

$$W(a,\tau) = \frac{1}{\sqrt{a}} \int_{-\infty}^{+\infty} f(t) \psi^* \left(\frac{t-\tau}{a} \right) \tag{1}$$

where the * represents the complex conjugate of the function. The CWT is simply a correlation of the signal, $f(t)$, with a scaled basis function $\psi^*(t)$. In general, the basis function is complex and is termed the "mother wavelet". The wavelet coefficient, $W(a,\tau)$ is also complex and can be represented in the Fourier domain as

$$\widehat{W}(a,\omega) = \sqrt{a}\, \hat{f}(\omega) \hat{\psi}^*(a\omega) \,. \tag{2}$$

The CWT is a linear operation and has an exact inverse transform given by the double integral

$$f(t) = \frac{1}{C} \int_0^{+\infty} \int_{-\infty}^{+\infty} \frac{1}{\sqrt{a}} W(a,\tau) \psi \left(\frac{t-\tau}{a} \right) \frac{da\, d\tau}{a^2} \tag{3}$$

where C is found from a Parseval-like integral

$$C = \int_0^{+\infty} \frac{\widehat{\psi}^*(\omega) \widehat{\psi}(\omega)}{\omega} d\omega \tag{4}$$

that requires the basis function to have zero mean for this integral to be bounded at $\omega = 0$. We use Morlet's wavelet (Goupillaud et al. 1985) in which

$$Re\big(\psi(t)\big) = \frac{1}{\sqrt{2\pi}} e^{-\frac{t^2}{2}} cos(2\pi\vartheta_0 t)$$

$$Im\big(\psi(t)\big) = \frac{1}{\sqrt{2\pi}} e^{-\frac{t^2}{2}} sin(2\pi\vartheta_0 t)\ . \quad (5)$$

As can be seen, Morlet's wavelet is a heavily damped sinusoid around t=0 allowing the scale parameter to be approximately interpreted as Fourier period (inverse frequency) in the CWT domain since we use $\vartheta_0 = 1$.

Figure 1 illustrates the use of the CWT and one particular thresholding scheme, hard thresholding, in removing noise from signal. The data come from a 2000lb explosion recorded at about 35km distance for a station within the IRIS experiment (details below). The raw time series data are transformed into the CWT domain to form a map of wavelet amplitude as a function of scale and time lag. The signal is seen both in the seismogram and in the wavelet map between 65s and 110s. This time-frequency representation (TFR) is a very intuitive way of viewing the characteristics of the signal that is seemingly buried by the noise. The signal is evident at scales shorter than 1s and is seen above the horizontal bands of lower frequency noise. Essentially, the map is a tool to view the signal in regions where the noise has much less amplitude than the signal. These areas of high signal-to-noise ratio (SNR) are of interest in partitioning the signal from the noise.

Partitioning can be accomplished several ways. In Figure 1, we show the results of "hard" thresholding. An estimate of the noise power is made in a time window before the first arrival of the event. This is then used with the following criterion to remove wavelet coefficients from the map. Coefficients are kept if they are greater than the mean plus 3 standard deviations (99.8% confidence level; Starck et al. 2010), otherwise they are set to zero. Mathematically, this is represented by

$$\widetilde{W}(a,\tau) = \begin{cases} W(a,\tau) & if\ |W(a,\tau)| \geq \beta(a) \\ 0 & otherwise \end{cases} \quad (6)$$

where

$$mean(|W(a,\tau)|) = \frac{1}{(t_2 - t_1)} \int_{t_1}^{t_2} |W(a,\tau)| d\tau \quad (7)$$

$$std(|W(a,\tau)|) = \left[\frac{1}{(t_2 - t_1)} \int_{t_1}^{t_2} (|W(a,\tau)| - mean(|W(a,\tau)|)^2\ d\tau \right]^{\frac{1}{2}} \quad (8)$$

and

$$\beta(a) = mean(|W(a,\tau)|) + 3\, std(|W(a,\tau)|). \quad (9)$$

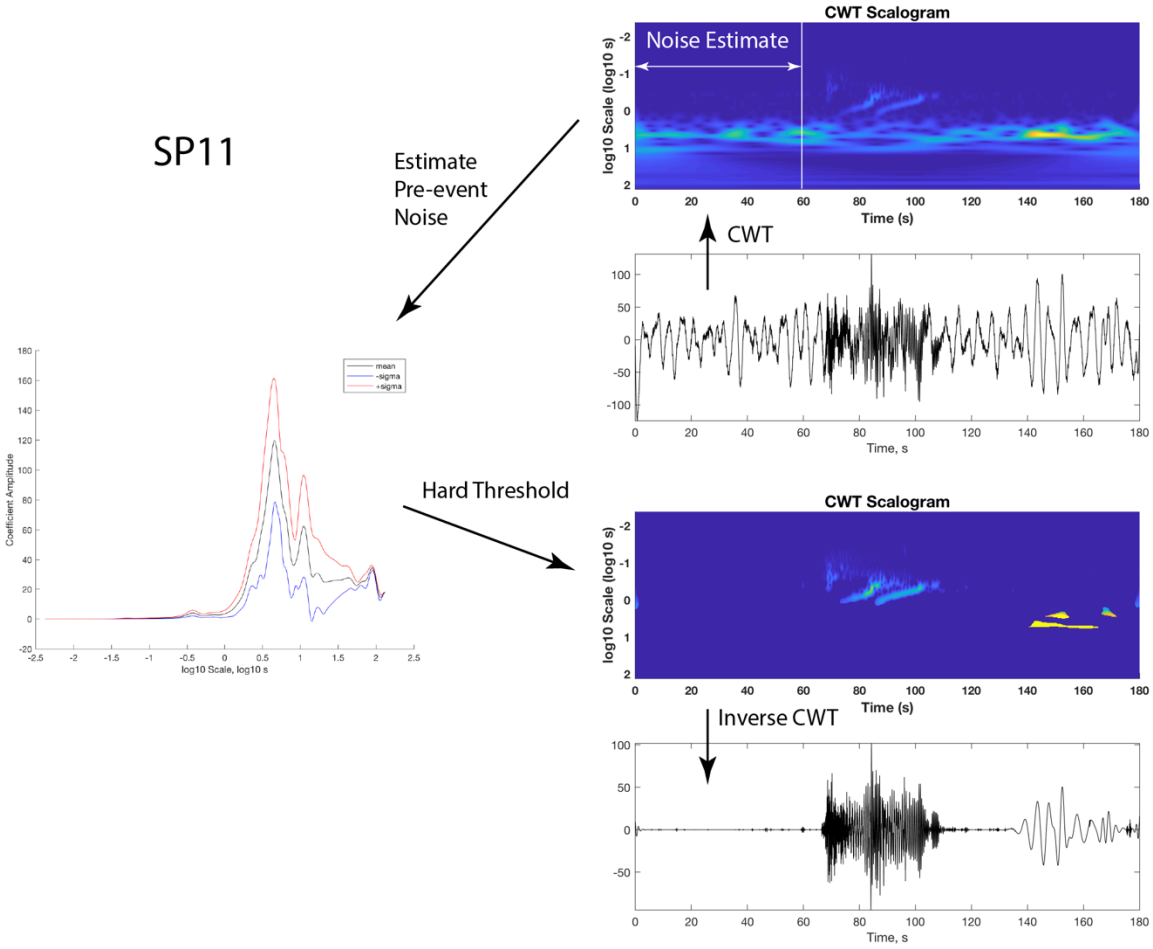

Figure 1 – An example of hard thresholding the CWT of an explosion signal buried in microseismic noise. *The signal (second panel from top) comes from shot point 1 near the IRIS experiment discussed below. The signal is transformed into the CWT domain to produce a map of wavelet amplitude (absolute value of the complex wavelet coefficient) vs time and scale. The signal can be seen between about 65s to 110s at scales less than 1s. An estimate of the noise amplitude is made by taking the mean of all wavelet coefficients at scale a within a 60s window before the event arrival. The mean amplitude vs wavelet scale is plotted to the left. Also shown in the plot are plus and minus one standard deviation. Wavelet coefficients in the map are then compared to the noise estimate and removed by the criterion discussed in the text. The CWT thresholded "scalogram" (third panel down) is then inverse CWT transformed to give the denoised seismogram (bottom panel). Note the spectacular reduction of noise in the time domain.*

The limits t_2 and t_1 represent the limits of the noise time lag window. Alternatively, thresholding can be done in a somewhat less severe manner by taking into account the amplitude of the noise in a "keep or shrink" process where the coefficients that survive are modified by the inferred noise level:

$$\widetilde{W}(a,\tau) = \begin{cases} sign(W(a,\tau))(|W(a,\tau)| - \beta(a)) & if\ |W(a,\tau)| \geq \beta(a) \\ 0 & otherwise \end{cases} \qquad (10)$$

where

$$sign\big(W(a,\tau)\big) = \frac{W(a,\tau)}{|W(a,\tau)|}\,. \tag{11}$$

Soft thresholding minimizes outliers in the noise and, in our experience, usually performs somewhat better than hard thresholding with seismic data.

3.1.2. Synchrosqueezing

Synchrosqueezing (SS) is a relatively new technique introduced by Daubechies and Maes (1996) and Daubechies et al. (2011) as a powerful tool for precisely decomposing and analyzing a signal. It can be classified as a time-frequency reassignment method aiming at a sharpened TFR by applying a post-processing reallocation on the original time-frequency representation. However, unlike classical reassignment methods (e.g. Auger and Flandrin 1995; Chassande-Mottin et al. 1997), SS is adaptive to different types of data, visually informative, and enjoys a simple and efficient reconstruction formula (Yang 2015).

At each time or space location, the SS process reassigns values of the TFR based on their local oscillation. The idea behind SS is that concentrating a spectrogram's energy around instantaneous frequencies will decrease spectral smearing, and thus sharpening the TFR, while still allowing its reconstruction. SS can be used to enhance many classical TFRs e.g. the synchrosqueezed continuous wavelet transform (SS-CWT) as in (Daubechies et al. 2011; Thakur et al. 2013; Iatsenko et al. 2015), the synchrosqueezed short time Fourier transform (SS-STFT) as in (Thakur and Wu 2011; Iatsenko et al. 2015), the synchrosqueezed wave packet transform (SS-WPT) as in (Yang 2015), the synchrosqueezed curvelet transform (SS-CT) as in (Yang and Ying 2014), and the synchrosqueezed S-transform (SS-ST) as in (Huang et al. 2015).

It has been shown that compared to the STFT and CWT, the SS-CWT has superior frequency resolution and for distinguishing oscillatory components of complicated signals (Thakur et al. 2013). Rigorous analysis has proven the stability and robustness of synchrosqueezing for analyzing 1D signals corrupted by noise or perturbations in the signal (Hou and Shi, 2012; Thakur et al., 2013).

Following Daubechies et al. (2011) the SS-CWT is performed in three steps. First, wavelet coefficients $W_y(a,\tau)$, of the recorded signal *y,* are calculated i.e. using equation (1). In the next step, a candidate instantaneous frequency $\omega_y(a,\tau)$ can be computed for wavelet coefficients of *y* at any point (a,τ)as:

$$\omega_y(a,\tau) = -\frac{i}{2\pi W_y(a,\tau)}\frac{\partial W_y(a,\tau)}{\partial t}\,, \text{ for } W_y(a,\tau) \neq 0. \tag{12}$$

The instantaneous frequencies are known as ridges in the TFR (Auger et al. 2013). In practice the very small wavelet coefficients $W_y(a,\tau)$ need to be removed to make the division operator numerically stable. SS squeezes the energy around these ridges (condensing the CWT coefficients at each time point along the scale axis) to decrease the smearing. To do this, in the last step, the information from the time-scale plane is transformed to the time-frequency plane, $(a,\tau)\rightarrow\langle\omega_y(a,\tau),\tau\rangle$. This operation is called synchrosqueezing and has been shown to improve the concentration of energy and, as a result, readability of the TFR (Daubechies et al. 2011). If the number of scales used in the CWT and the sampling frequency are N and *sf* respectively, frequencies on the SS-CWT would be $\omega_l = lsf/N,\ l\in[1,N]$ because $W_y(a,\tau)$is calculated at discrete values a_k. The CWT coefficients within the frequency range $\Delta\omega=\omega_l-\omega_{l-1}=sf/N$, will be added up to the center frequency ω_l to construct each instantaneous frequency. Hence, the synchrosqueezed transform is defined as:

$$T_y(\omega_l,\tau)=\Delta\omega^{-1}\sum_{a_k|\omega(a_k,\tau)-\omega l|\le\Delta\omega/2} W_y(a_k,\tau)a_k^{-3/2}\Delta a_k \quad , \tag{13}$$

where $\omega_l$is the l th discrete frequency, $a_k$is the *k* th scale, and $\Delta a = a_k - a_{k-1}$. We can recover individual component y_k, from the T_y by integrating the coefficients over frequencies ω_l, that correspond to the k_{th} component. Following (Thakur et al. 2013) let the $l\in L_k(t)$ a small frequency band around the ridge of k_{th} component in the SS-CWT. This band can be estimated using a standard least-square ridge extraction method (e.g. Carmona, et al., 1997) or defined manually. Because $y_k$is real, then we will have:

$$y_k(t)=2C_\psi^{-1}\Re e\Big(\sum_{l\in L_k(t)} T_y(\omega_l,t)\Big)\,. \tag{14}$$

Doing so, one can decompose a signal into its constituent components. It is clear that the highly structured TFR provided by synchrosqueezing (Figure 1) can be exploited for classical signal processing applications such as denoising (Auger et al. 2013).

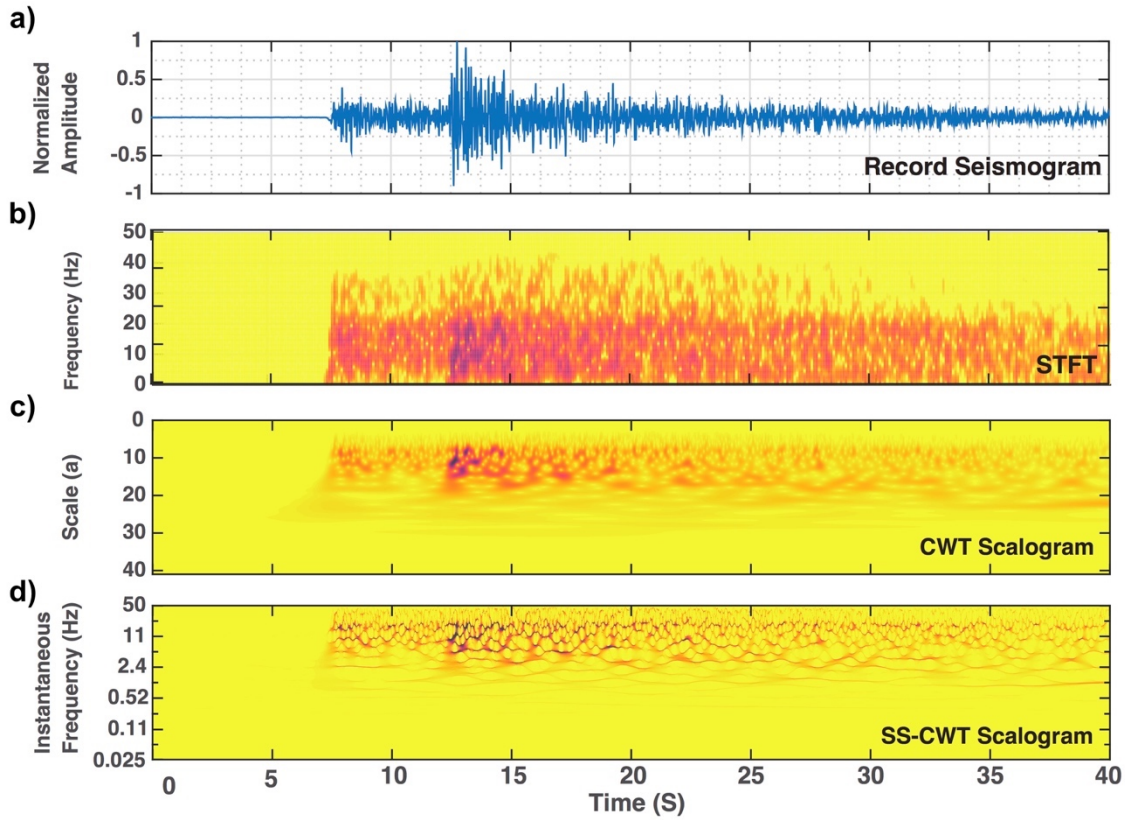

Figure 2 - The top panel shows a high SNR vertical component accelerogram for a M3.5 event recorded at station HALT, TN, in the New Madrid Cooperative Seismic Network. The next panels downward show the STFT, CWT, and SS-CWT, respectively, representing TFRs of the same signal. *The variable length of* ψ *leads to a relatively higher time-frequency resolution of the CWT (c) compared to the STFT (b). However, it still displays spectral smearing due to the finite size of the operator. Note the sharpened TFR obtained by the SS-CWT (d).*

3.2. Time-Frequency Denoising Studies

This work has culminated in 4 publications concerning Time-Frequency Representations of seismic data. The basic idea behind all techniques involves manipulation of a two-dimensional mapping where the location of a "signal" is discriminated from "noise" on a plane consisting of complex amplitudes determined from the transform of a short time window of seismic data. A common transform is the short time window Fourier transform (STFT) but other transforms, such as the continuous wavelet transform (CWT) and the synchrosqueezed CWT may represent the time series data in more compact form (e.g., Figure 2). The STFT is the basis for the common spectrogram where short running time windows of the data are Fourier transformed and then the amplitude or power spectra are plotted as a function of time. The CWT may be implemented with a choice of different wavelet functions and is computed in a similar manner to the STFT in which a short time window is transformed with wavelet coefficients at different scales being plotted against time. The synchrosqueezed CWT (SS-CWT) represents another processing step where the CWT is modified by assigning the energy of closely adjacent wavelet coefficients to ridges

in the CWT time-scale map. Both the CWT and the SS CWT attempt to represent the seismic signal (and the noise) by the smallest number of coefficients.

The transformed signal can be manipulated by a number of techniques to characterize both signal and noise and then to remove either. Once a quantitative characterization is obtained for properties of the noise, it can be removed by applying a threshold criterion to sections of the time-scale map. The processed time-scale map is then inverse transformed to obtain the denoised signal.

In Mousavi, Langston and Horton (2016a), an algorithm was developed around the SS-CWT for the purpose of detecting microtremors within noise. In this algorithm, the time-scale CWT map for small events embedded in noise was partitioned based on the character of high scale (low frequency) background noise and low scale (high frequency) microtremors. This part is most analogous to highpass filtering where the higher frequency part of the map is treated separately from the low frequency part. Assumptions involve considering an event to be localized at small scales and in time and to have larger wavelet coefficient amplitudes. Noise is characterized by low values of wavelet coefficients but by larger numbers of coefficients. After determining the boundary of the high scale noise and low scale signals, the map is split and synchrosqueezed to reduce the number of wavelet coefficients needed to describe both the noise and the signal. Using a pre-event time window, the statistics of the noise in the signal and noise parts of the map is determined. Using these statistics, "soft-thresholding" is applied to the high scale noise segment and the noise attenuated across scale by dividing by the high amplitude wavelet coefficients. A detection function is then constructed to detect the high amplitude signal components by computing the energy from a Parseval-type computation of the wavelet coefficients as a function of time.

Block thresholding was explored by Mousavi and Langston (2016a) incorporating only the signal's CWT. First the CWT time-scale map is computed for a time series. Gaussian noise is then detected in the CWT through computation of the kurtosis (HOS or higher order statistics). This noise is then removed from the CWT map by a statistical test. The data are then processed scale by-scale as a function of time by determining an optimum time block length using an estimate of the strength of the signal's wavelet coefficients compared to the noise. The "hybrid" aspect of this process is having different block lengths for the coefficients at each scale and attenuating wavelet coefficients based on adaptive parameters that change with time and scale. The attenuated noise coefficients are then subject to an additional Weiner filter and transformed back into the time domain. Remarkably, all of these wavelet coefficient manipulations preserve relative amplitudes and particle motions of seismic phases in the three component data. Use of the CWT is relatively computationally intensive in these previous techniques compare to a STFT.

Mousavi and Langston (2016b) incorporated the STFT to compute the time-frequency map and then applied an adaptive block size and threshold value to remove the noise. Noise level is estimated by assuming that the signal is larger than the noise and by tracking minima on the time-frequency plane. There is a recursive process for determining the noise variance in one section of the plane compared to adjacent sections. Once the statistics of

the noise is known, the Fourier coefficients of the noise in one block can be attenuated by using the noise estimates in adjacent blocks. The denoised STFT is then transformed back into the time domain. Although this method does not preserve waveform as well as the previous methods, it is almost 2 orders of magnitude faster in computation time and is appropriate for fast detection algorithms.

Mousavi and Langston (2017) combined general cross-validation (GCV) thresholding in the synchrosqueezed domain to produce a method that uses robust assumptions about the noise level. First the level of Gaussian noise is estimated from the kurtosis of the time series and then eliminated. Synchrosqueezing the remainder converts the signal TFR into undulating ridges (Figure 2). Signal is chosen by the GCV algorithm by choosing that portion that is most "ridge-like". This kind of analysis favors signals that are locally harmonic so the instantaneous frequency looks relatively continuous. Inverse transforming this TFR after thresholding yields either a denoised signal, if wanted, or a designaled noise field, if wanted. The method performed quite well for a variety of data types including ocean bottom seismometer data, microseisms, and local/regional earthquake data.

3.3. BCseis MatLab Software

One theme that occurred within these studies was the issue of algorithm speed vs fidelity of the denoised signal. More operations on a data trace and its TFR increased the number of processor cycles. Higher fidelity noise reduction with extra processing steps, like using the SS-CWT with GCV, significantly increased processing time that made denoising array datasets tedious. Another odd drawback of these studies was the relative difficulty in obtaining an intuitive view of the signal and noise on the TFR plane. Gaining insight into the signal and noise is routinely done by a seismic analyst simply by assuming various bandpass filters and observing their effect on the data time series. Characteristics of the noise can be quickly seen and appropriate filters for the task at hand can be used to consistently process the data.

For these reasons, we wrote an interactive Graphical User Interface (GUI) to take single trace data in Seismic Analysis Code (SAC) format and then perform various interactive processes on the TFR. This gives a much-needed way of testing various simple processing schemes for particular waveforms quickly and gaining intuitive knowledge about the signal and noise. Once the data from one or more traces have been studied, parameters can be used with an in-line MatLab function "BCseis_process" to consecutively process many traces within a large dataset. The software is provided separately and contains a series of built-in "Help" pages to illustrate its use (Figure 3).

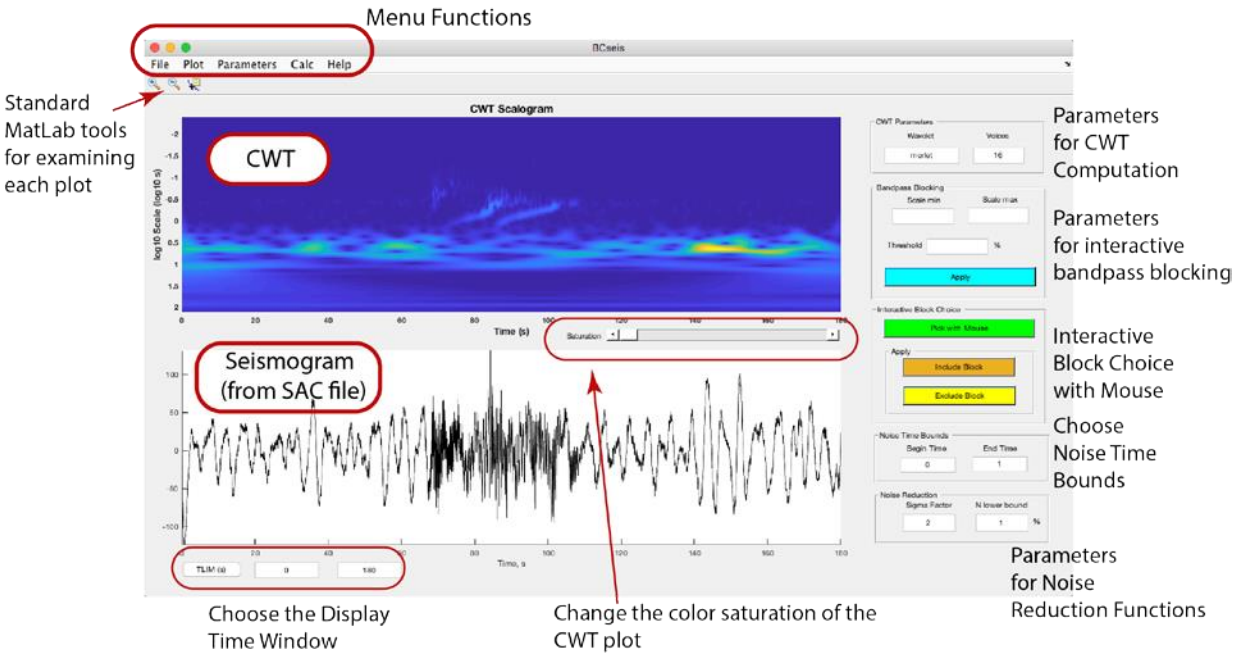

Figure 3 – An overview of the interactive MatLab GUI, BCseis. *A seismic trace in SAC format is chosen from a file menu and read into the program. The CWT is computed using a choice of 4 different wavelets. The resulting TFR can then be investigated using interactive block thresholding, bandpass filtering, hard thresholding, and soft thresholding. Noise characteristics are investigated using user-determined time intervals to compute noise statistics. These noise statistics are used in the hard and soft thresholding process.*

Figure 1 shows an example of hard thresholding using figures generated by BCseis for an AFTAC explosion recorded by the IRIS experiment. A very satisfying and remarkable by- product of this software was the ability to take a seismic signal apart into obvious component pieces that can be further analyzed. A complex seismogram consisting of several phases can be separated into meaningful wave trains particularly when several different surface wave modes are part of the composition. Figures 4a and 4b demonstrate this ability for the SP11 2000lb shot that is displayed in noisy form in Figure 1. After denoising using the soft threshold method, the vertical component at station 5014 shows virtually no pre-event noise. (This is not a synthetic seismogram!) A careful look at the waveform and the CWT amplitude plane shows a small local earthquake superimposed on the dispersed wave train near 95s time. Using our interactive software tool, the small event is located on the CWT plane, encompassed with a polygon using the computer mouse, and then removed by setting all wavelet coefficients within the polygon to zero. The inverse CWT shows that the event has been removed from the wave train. The same process is then used in reverse to choose the fundamental mode (continuation of Figure 4a) and the first higher mode (Figure 4b) by zeroing out all other coefficients except those chosen within the polygons. At this point both modal seismograms can be analyzed for group velocity dispersion using standard methods and the dispersion modeled to obtain an Earth model.

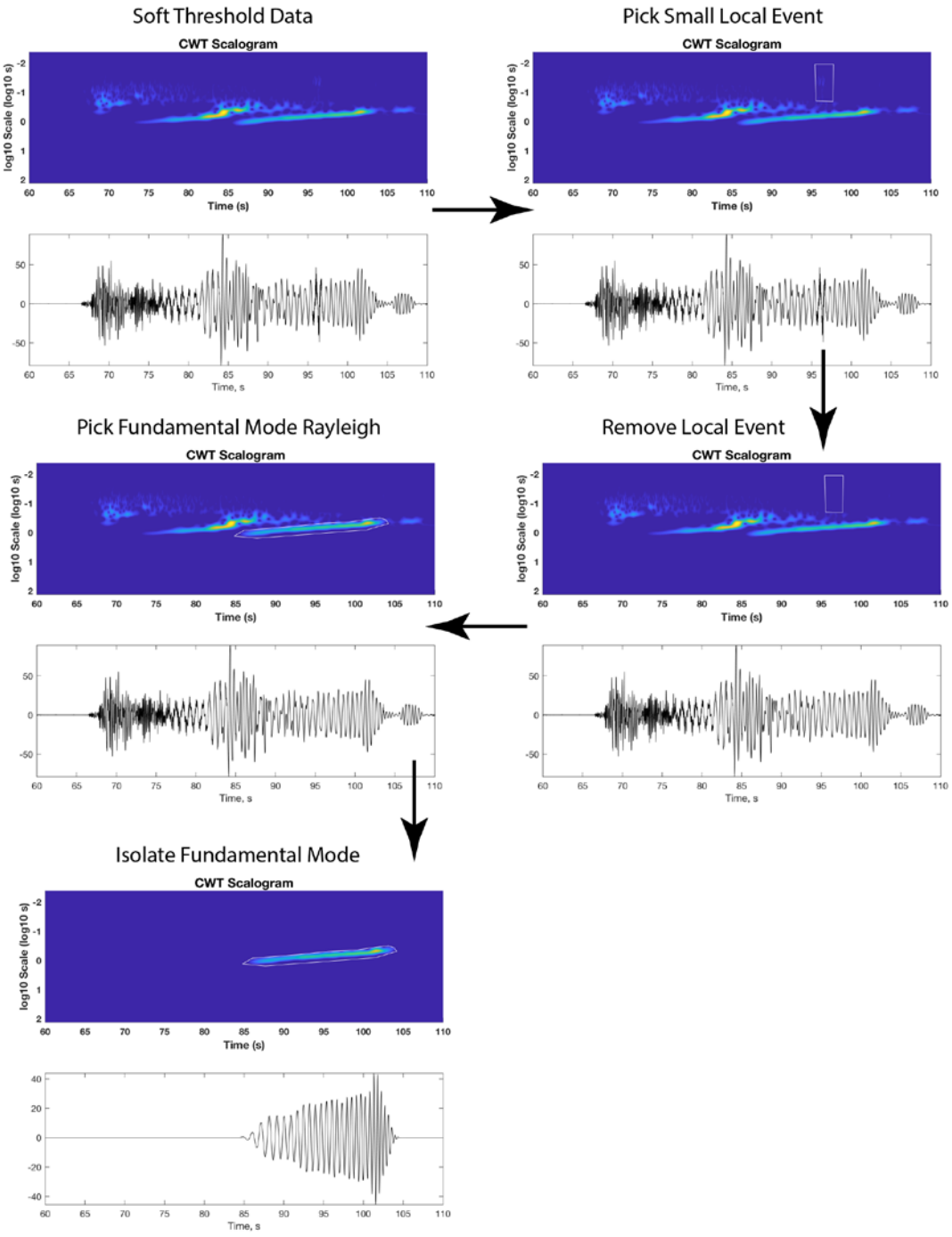

Figure 4a – Block thresholding a small local event from the seismogram of SP11 at station 5014 and separating the fundamental and first higher mode wave trains. *The original seismogram is shown in Figure 1. After soft thresholding, the resulting waveform is clearly seen in the time domain with a distinctive signature in the CWT domain as well (upper left pair of CWT/seismogram panels). A small high frequency local earthquake is seen to interfere with the Rg phase near the 95s mark. The event can be seen in the CWT amplitude plane so is isolated by picking block boundaries (with the computer mouse) and removed by zeroing these wavelet coefficients (from upper right to middle right). Next, the fundamental mode Rayleigh wave is manually chosen by*

defining a polygonal block around the dispersed, high-amplitude wavelet coefficients on the CWT amplitude plane (middle left panels). All other wavelet coefficients are zeroed out to leave the fundamental mode and the inverse CWT computed to show only the fundamental mode waveform. The same process can be done to delineate the first higher mode in the CWT amplitude plane and to separate it from the seismogram (Figure 4b).

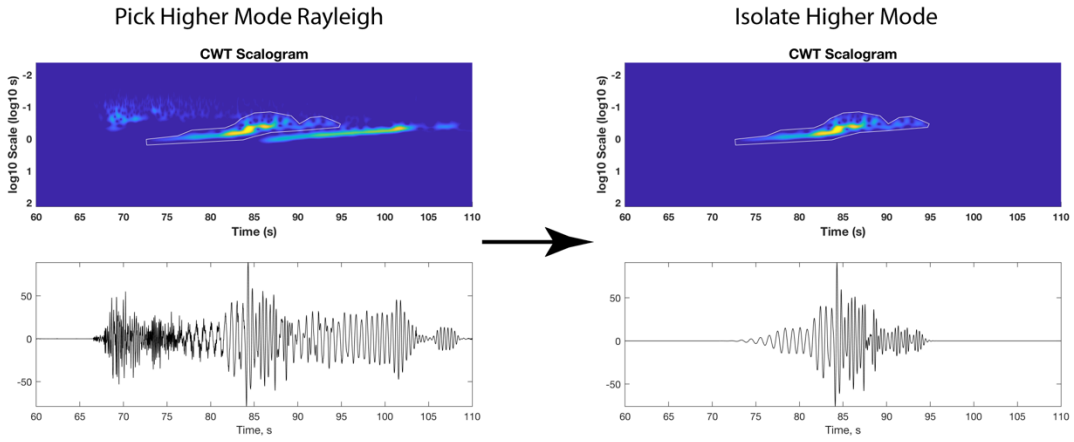

Figure 4b – Separating the first higher mode Rayleigh wave from the vertical component of station 5014 for shot point 11. *An irregular polygon is picked in the CWT amplitude plane (left panels). All other wavelet coefficients are set to zero and the inverse CWT taken to obtain just the higher mode (right panel).*

3.4. Application of Block Thresholding Methods to Seismic Array Data

3.4.1. Study of Source Physics Explosions Recorded at NVAR (Mina, NV)

We applied noise reduction methods developed for single three-component sensors to seismic data recorded by regional seismic arrays. A study has been completed for investigating the application of Block Thresholding to the problem of increasing the Signal-to-Noise ratio (SNR) and improving array responses for two explosions of the Source Physics Experiment (SPE) at the Nevada National Security Site (NNSS) recorded at the International Monitoring array NVAR, Table 1. The location of the shot borehole is the same for both explosions and NV01 in the NVAR array (Figure 5) is 239km from the shots with a back-azimuth to the sources of 123.5º.

Table 1 – SPE Explosions investigated at NVAR (from Snelson et al. 2013)

Shot Name	Depth (m)	Yield (Kg)	Origin Time (UTC)
SPE-1	54.9	87.9	3 May 2011 22:00:00.01136
SPE-3	45.8	905	24 July 2012 18:00:00.44835

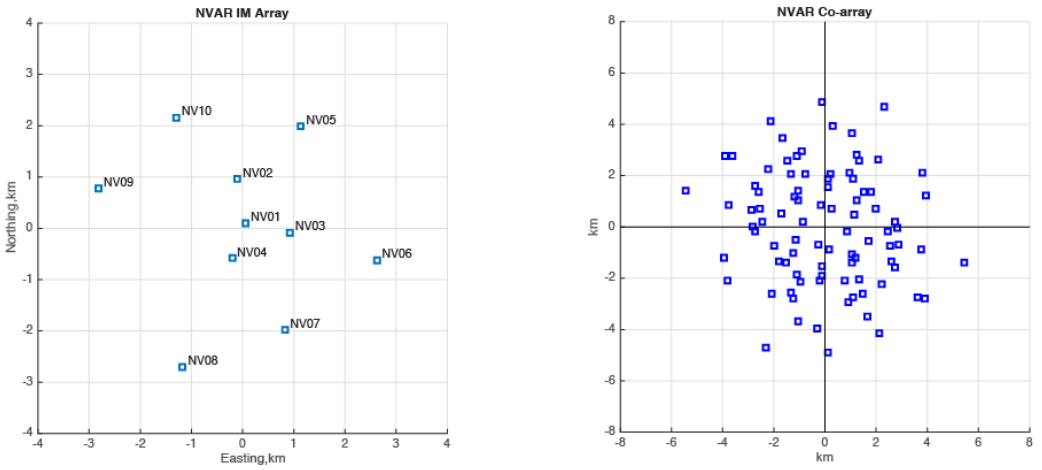

Figure 5 – Geometry of the first two rings of the NVAR array (*left*) showing the stations used in the array analysis. The *right* panel shows the co-array diagram for NVAR. *The co-array is the collection of all distances and azimuths between stations of the array taken two at a time. The co-array indicates the spatial sampling of a seismic wave as it sweeps across the array.*

We are interested in two things in this data analysis experiment. The first is to see if applying the block-thresholding scheme improves the array response in any way for the larger of the two events, SPE-3. The second goal is to identify the signal from SPE-1 at NVAR using Time-Frequency Representations. This experiment brings up several interesting issues that aren't related to the noise reduction schemes, per se, but point to useful research directions in detecting very small events with arrays.

Noise was estimated using the first 30s of record before the P wave arrival of event SPE-3 and used to correct the data using the soft thresholding method (Figure 6). The P and S wave signals clearly have improved signal-to-noise ratios. A look at the TFR plane shows that portions of the signal and noise are clearly separated, explaining the excellent reduction in pre-event noise from soft thresholding (Figure 7). Nevertheless, we find that the noise thresholding has an unusual effect on the beam forming ability of the array.

It is first useful to investigate the expected, ideal broadband slowness response of the NVAR array (Nawab et al. 1985) (Figure 8). NVAR is composed of short-period S-13 vertical seismometers arranged in two rings (Figure 5). A third ring of three broadband seismometers is deployed about 5 km from the center, but these stations are not considered

here. The SPE-3 explosion data are effectively bandpassed between 1 and 5 Hz both by the preprocessing and the denoising. Two array responses are shown in Figure 8 that presage the data analysis. Both show focused high amplitude power maxima with small side lobes.

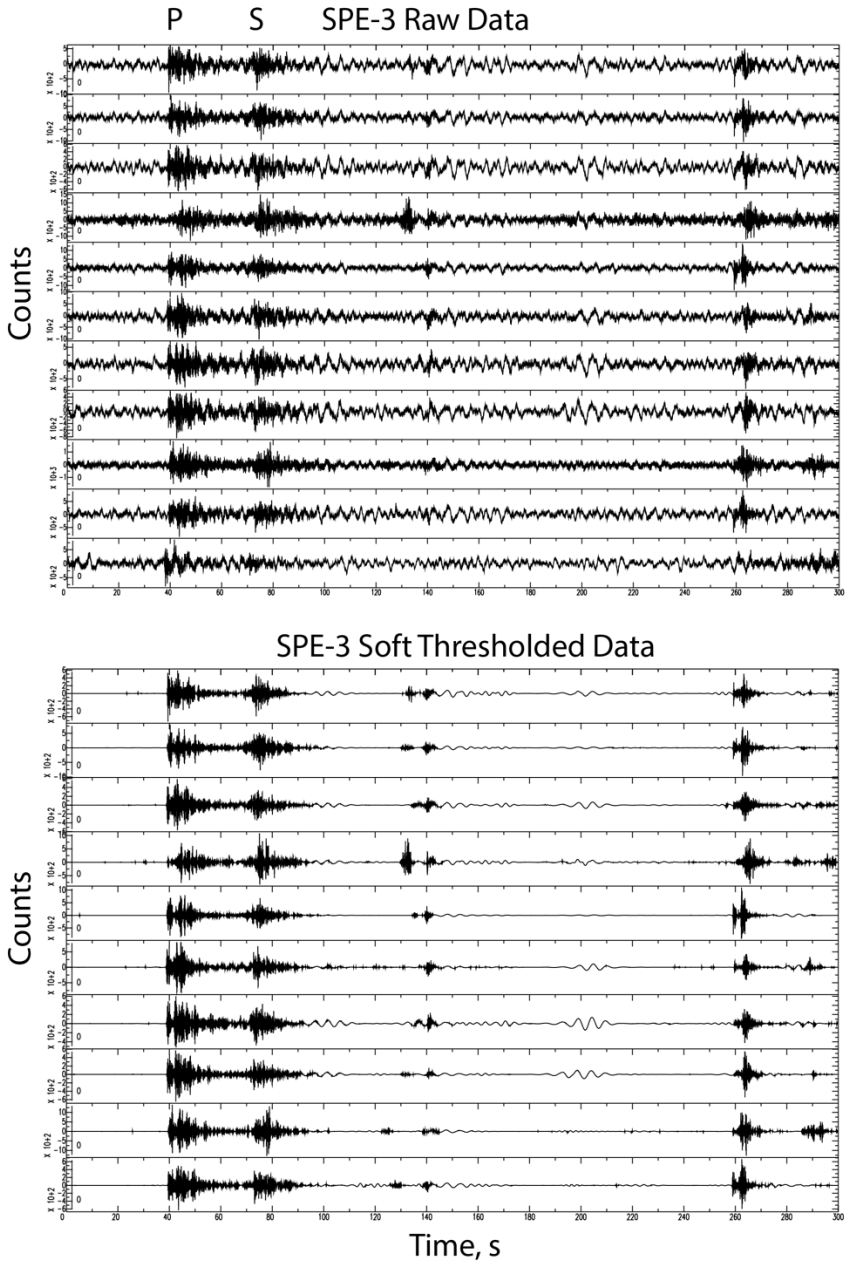

Figure 6 – Raw (top) and soft thresholded waveform data (bottom) for the SPE-3 explosion recorded at the NVAR array. *The first 30s of record at each station was used to estimate the statistics of the noise field for removal using soft thresholding. The processed waveforms clearly have improved signal to noise ratios for the major P and S phases after thresholding. At least 2 other closer local earthquakes are seen after thresholding with waves arriving near 140 s and 250s.*

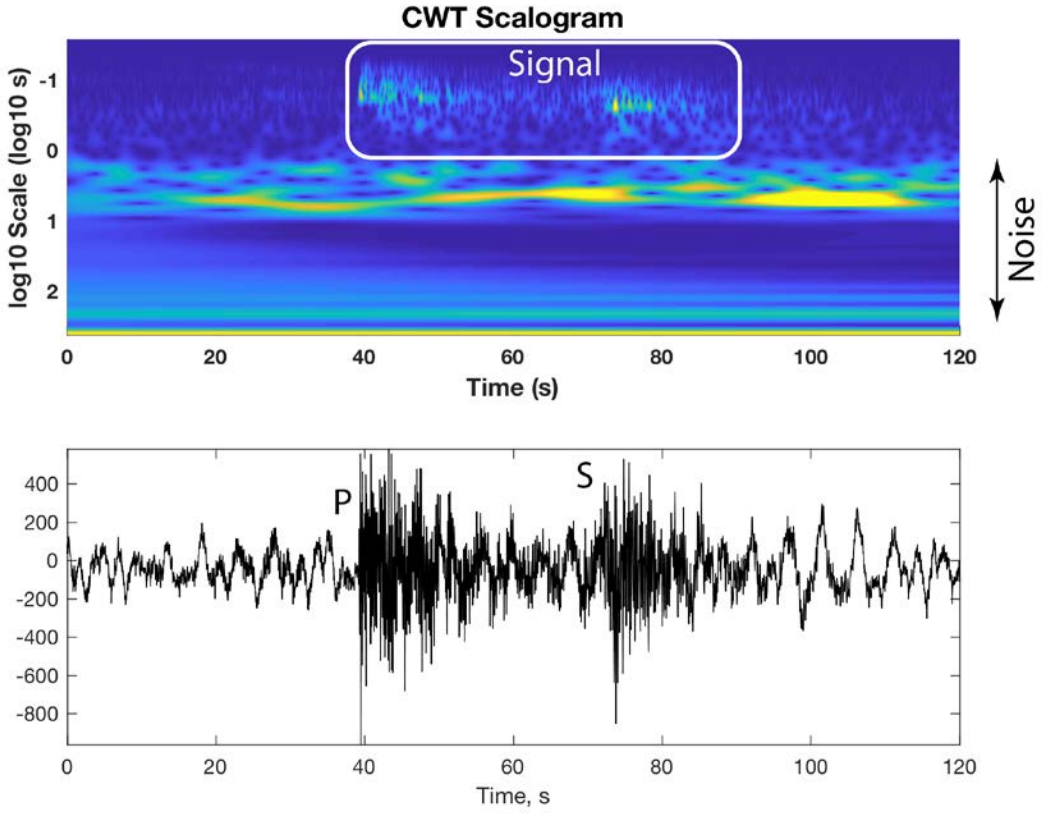

Figure 7 – Vertical component time series at NV01 (bottom) and its CWT (top). *Portions of noise and signal are clearly separated on the CWT plane. However, notice that noise for scales of 1s and less (0 to less than -1 in log units) exists before the signal arrival. The signal will be reduced by this amount of noise on the average.*

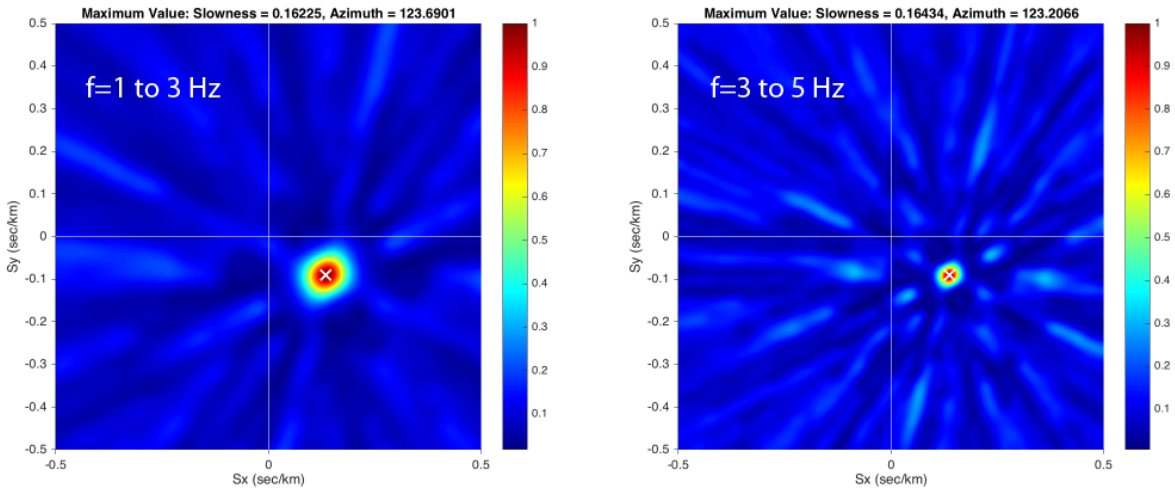

Figure 8 – Theoretical broadband slowness plane-wave responses for a wave with phase velocity 6 km/s arriving from a back-azimuth of 123.5°, modeling the P wave group of arrivals from SPE-3. *Frequency bands of 1 to 3 Hz and 3 to 5 Hz are assumed in the calculations. These responses incorporate all 10 stations of the center and two rings of NVAR.*

Broadband responses for the raw and thresholded data (Figure 9) show that beamforming is degraded for the thresholded data when three standard deviations of noise is used in the threshold criterion (i.e., in equation 9). The backazimuth determined from the raw data is almost exactly the correct back azimuth of 123.5^o. The data used in beamforming from thresholding at 3 times the standard deviation clearly degrades the beam. If a less stringent, one standard deviation is used for thresholding, then more low frequency signal is recovered to give the correct backazimuth. However, in this case, there is no real advantage to use denoising before beam forming; the patterns are very similar.

Results for 3 to 5 Hz are highly aliased for all cases. Waveforms, both raw and denoised, correlate poorly across the array so do not form adequate beams. The horizontal wavelength of these regional P waves should be approximately 1-2 km for a P wave phase velocity of 6 km/s in the frequency band of 3-5 Hz. Waves de-correlate even across the inner ring of NVAR suggesting that it might be useful to have a spatially dense, high frequency array to observe local and regional waves at high frequency.

The SPE-1 shot was an order of magnitude smaller than SPE-3 in yield (Table 1) and is a challenge for detection in the data (Ford and Walter, 2015). We applied the soft-thresholding algorithm to the NVAR data in attempt to detect the signal with and without array beamforming.

At first, candidate signals were observed at stations NV01 and NV02 within roughly the correct time windows but signals were not observed at the other stations. A closer look at the NV01 and NV02 data showed that the apparent explosion P or S arrivals did not match the relative times observed for SPE-3. Straightforward application of our denoising techniques did not pull the explosion from the data.

The implementation of the soft thresholding method improved the visual SNR of the SPE-3 explosion dataset yet the resulting broadband array analysis showed no significant differences compared to simple bandpass filtering of the data. The major issue with the array analysis was heterogeneous earth structure that served to de-correlate the P and S waveforms at frequencies higher than 3 Hz. In an effort to investigate this problem a large teleseism was obtained from the IRIS data center for NVAR and it was found that even 3 to 5 Hz teleseismic P waves also de-correlated across the array.

This suggests that detection of small, high-frequency regional sources by an array would be better served by building denser arrays with small apertures to sample the short wavelength portion of the wavefield. Although wave scattering will be an increasingly important problem at higher frequency, small apertures with dense sampling will allow greater correlation of the local wavefield and, hence, better detection capabilities.

This initial look at the use of one de-noising technique yielded a neutral result; soft thresholding and simple bandpass filtering gave the same result when using the processed data in broadband frequency-wavenumber analysis, particularly if the thresholding criterion was weak. However, the exercise was quite useful since it pointed out several characteristics of weak signals that swim in a sea of noise from a time-frequency representation (TFR) map point of view. Sources can often be easily seen in the TFR if they are separated from areas of noise. Time windows and frequency/scale bands can be interactively defined and be blocked out for special analysis in a very similar way of simply trying different types of bandpass filters as in spectral analysis. This could be a useful

hands-on method to learn about individual signals and arrays of signals before designing and implementing automatic methods of noise reduction.

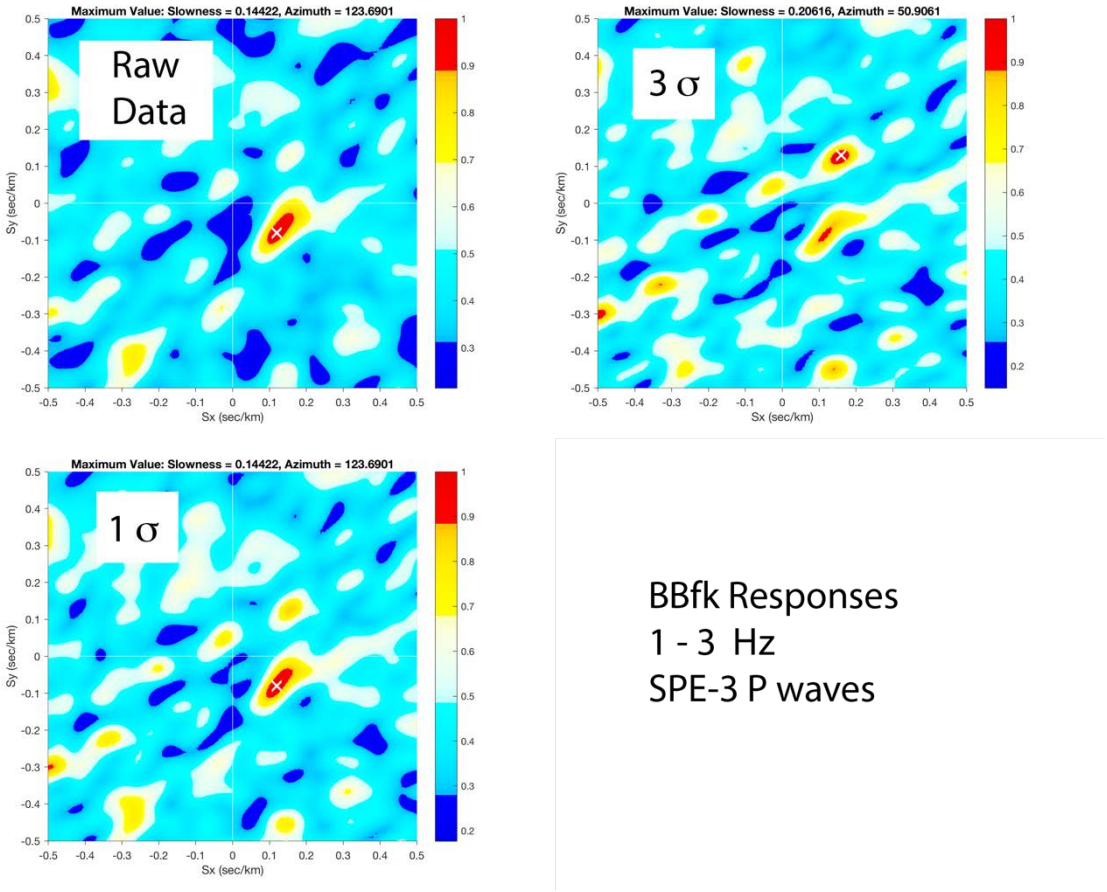

Figure 9 – Comparison of BBfk responses in the frequency band 1 to 3 Hz for the raw data for SPE-3 at NVAR (top left) and soft thresholded data (top right and bottom left). *Data for the P wave is windowed between 35 and 55s for the BBfk calculation. The top right panel shows the beam pattern for a soft threshold criterion of the mean plus 3 times the standard deviation of the noise distribution. The bottom panel is for data that have been thresholded using the mean plus one standard deviation.*

3.4.2. Study of AFRL Explosions Recorded by the IRIS Community Wavefields Experiment

The IRIS Community Wavefields Experiment (Figures 10 and 11) was designed by an ad hoc committee of academics as a passive seismic experiment to record the large amount of induced seismicity in northern Oklahoma and as an active vibroseis experiment that was to be run along the linear profiles. Unfortunately, the vibroseis experiment did not take place because of county permitting restrictions. However, passive recording of seismicity was very successful with literally thousands of local and regional earthquakes being recorded.

The P.I. was involved in designing three parts of the experiment. One part was a broadband regional array with an aperture of about 6 km in the Golay 3x6 configuration (Figure 11). The linear profiles and the P.I.'s 7-level gradiometer were composed of 5 Hz, three-

component ZLand Fairfield Nodal seismometers. In addition, the linear profiles were densified where they cross each other to form an additional two high frequency regional arrays in "cross" formations. We compared the broadband Golay array response to a dense cross array formed by eastern intersection of the linear profiles. The Golay array is representative of a typical, relatively sparse regional array similar to many CTBTO arrays although it is an unconventional geometry with no center elements. The "cross" array highly oversamples the wavefield and is ideal for examining array relative performances.

We take advantage of a second data source associated with the IRIS experiment. Cleat Zeiler from AFTAC, Wyoming office, performed an explosion source experiment on 14 July 2016 and 16 July 2016 during the nodal seismometer deployment. Twelve explosions ranging from 2000 lbs to 250 lbs (Table 2) were detonated at three locations in northern Oklahoma (Figure 12). This data set is ideal for evaluating array performances, examining the nature of seismic phases from local explosions, and understanding ambient noise and location of signal in Time Frequency Representations of the data.

We found that array detection of high frequency regional phases is best done with densely spaced high frequency arrays validating the assertion made in the NVAR study where extreme de-correlation was observed between sensors. Clearly, using a dense high frequency array outperforms a broad band, relatively sparse, regional array (Figures 13 and 14).

We also performed a test of the CWT thresholding techniques on reducing noise and recovering explosion waveforms (Figure 15). Shotpoints 11 through 14 (Table 2) were closest to the experiment. Both hard thresholding and soft thresholding produced superb noise reduction revealing highly similar waveforms. Clear detections with P wave slownesses and backazimuths were obtained using cross array data for SP11 and SP12, at about 35km distance, and only SP31 at 67km distance. The smaller shots in each group were dominated by microseisms consisting of local anthropologic noise sources and microearthquakes (Figure 16).

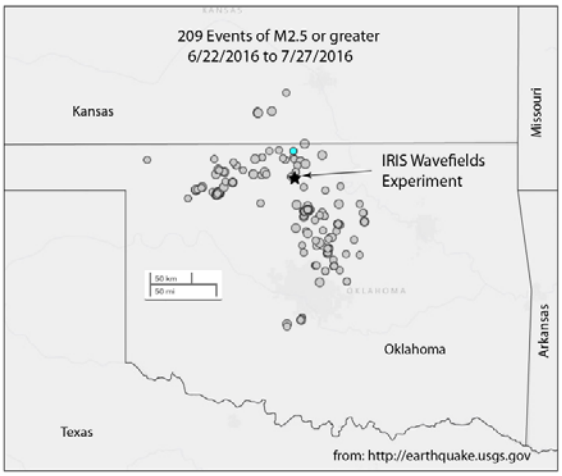

Figure 10 - Index map of the location of the IRIS Wavefields Experiment (star) and 209 earthquake events of M2.5 or greater during the time interval of June 22 to July 27, the duration of the nodal seismometer deployment.

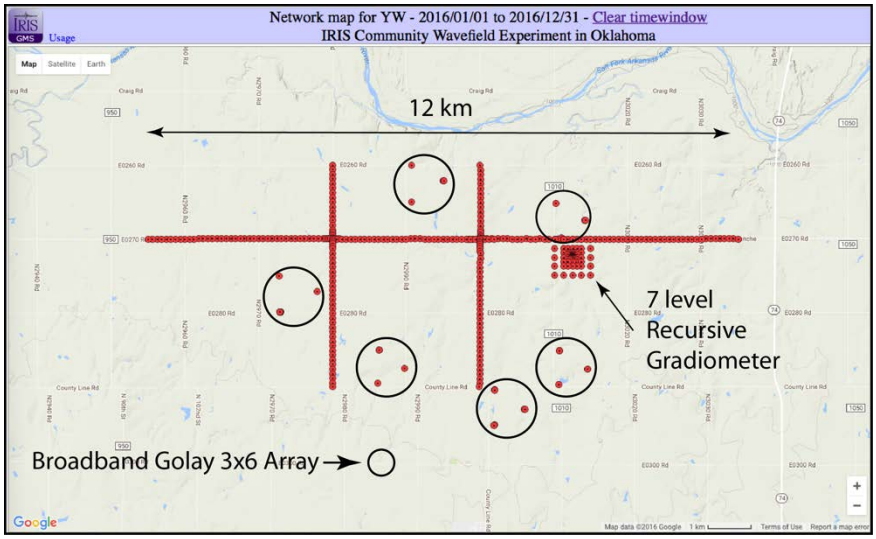

Figure 11 – GMAP figure (from IRIS website) showing the different elements of the seismic experiment. *247 three-component nodal seismometers were deployed in two NS 5 km lines and one EW 12 km line. 112 three-component 5Hz nodal seismometers were deployed in a 800x800m 7 level, nested gradiometer configuration. 18 broadband seismometers were deployed as a "Golay 3x6" array with an approximate aperture of 6km (circles enclosing subarrays of 3 stations each). 9 infrasound instruments were sited with 9 of the broadbands to help in discriminating acoustic signals that might be recorded seismically.*

Table 2 – Shot Information for the AFRL Experiment (courtesy of Cleat Zeiler, 2017)

Shotpoint #	Latitude	Longitude	Elev. (m)	Date	Time	Nominal Charge Size (lb.)	Comments
11	36.825026	-97.956602	343.8	14-Jul	14:26:00	2000	
12	36.824767	-97.956618	341.4	14-Jul	14:15:00	500	
13	36.824747	-97.956251	341.9	14-Jul	14:05:00	250	
14	36.825053	-97.956182	343.1	14-Jul	3:26:00	250	shotgunned
21	36.551591	-97.517971	304.6	16-Jul	0:37:00	2000	
22	36.551312	-97.517956	303.2	16-Jul	0:25:00	500	
23	36.551303	-97.517588	305.1	16-Jul	0:14:00	250	
24	36.551302	-97.517242	304.1	16-Jul	0:04:00	250	
31	36.113566	-97.248696	300.3	14-Jul	15:12:00	2000	
32	36.11365	-97.248307	300.1	14-Jul	15:02:00	500	
33	36.113896	-97.248479	299.8	14-Jul	14:50:00	250	
34	36.113816	-97.248777	301.3	14-Jul	3:40:00	250	geysered

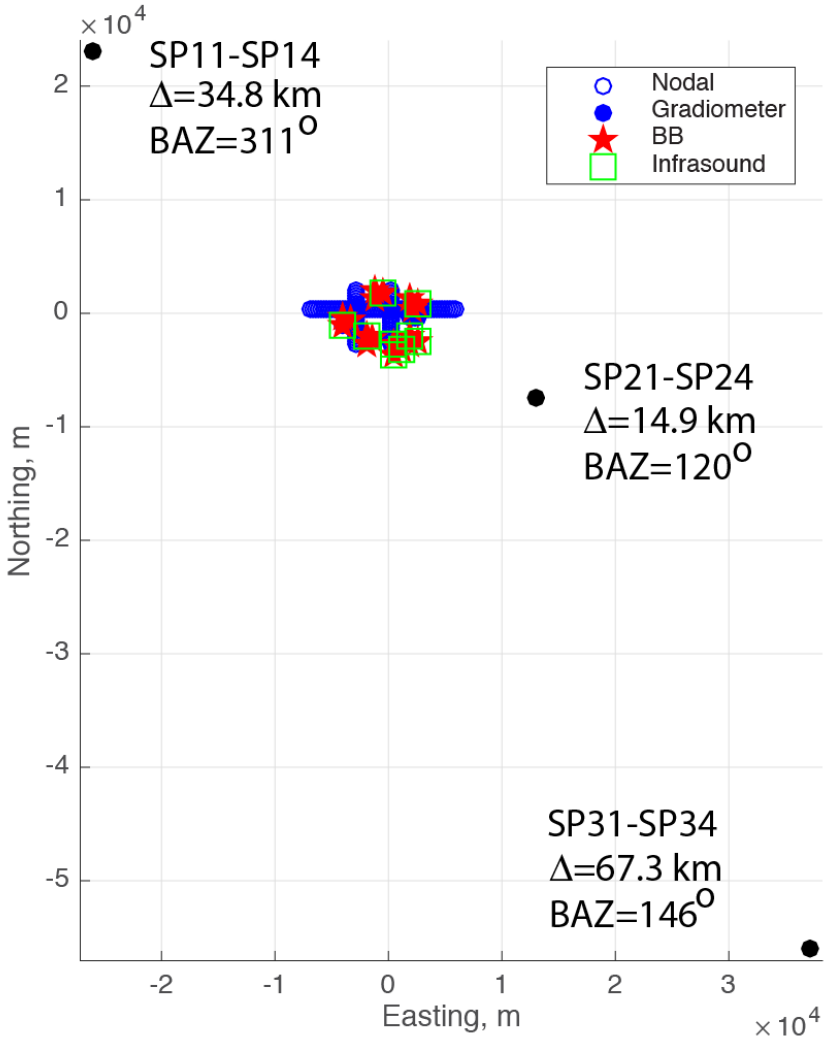

Figure 12 – Source – Array geometry for the AFTAC explosion experiment. *The IRIS Wavefields Community Experiment is shown near the origin. Shot locations are shown by filled circles with distance and backazimuth from the array origin as noted. Source parameters are listed in Table 2.*

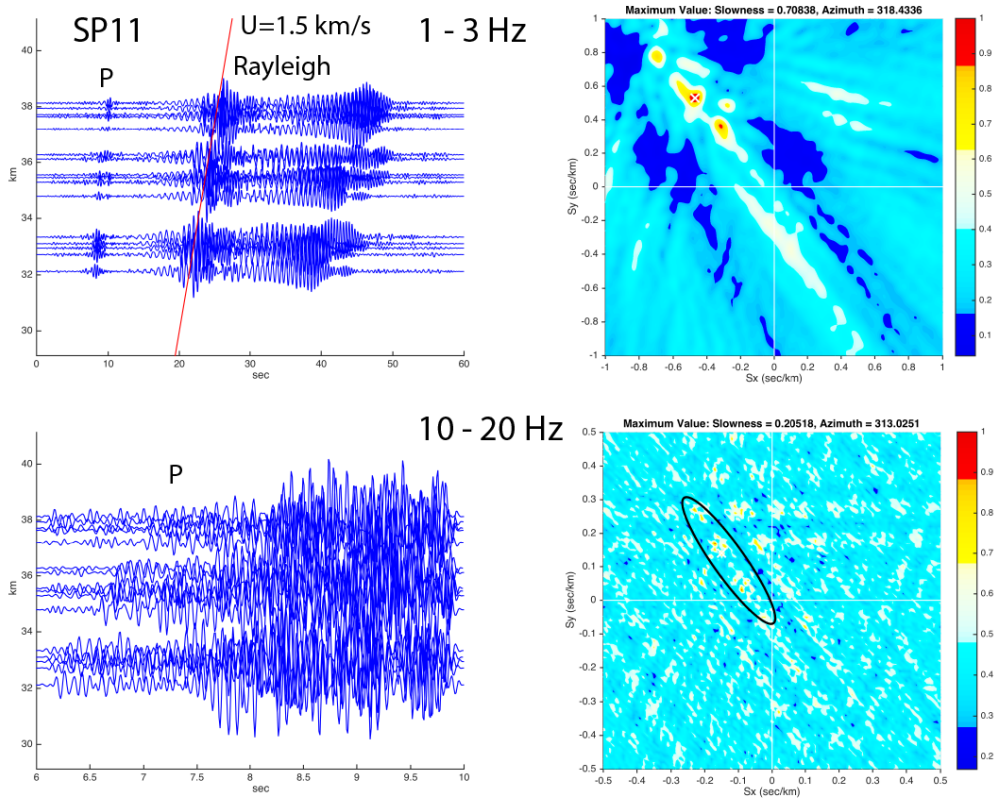

Figure 13 – Results of array analysis of SP11 vertical component data from the Golay array. *The data (upper left) filtered to 1-3 Hz show clear P and multimode Rayleigh waves. BBfk of this window (upper right) yields good resolution for determining the slowness and back azimuth of the Rayleigh waves. P waves in the band 10-20 Hz are well recorded (lower left) yet do not show up well in the BBfk plot (lower right). Even so, the correct azimuth and plausible slowness is obtained from the Golay array data. (A detailed look at the array response shows several peaks of comparable amplitude, however.)*

The SP31 shot case provides an interesting study in array capability and detection with and without noise reduction (Figures 16 and 17). The data were processed using the soft thresholding method in this numerical experiment. Waveforms clearly show P wave and Rg wave groups but also reveal other high frequency seismic waves. Many of these waves are probably anthropogenic since they have very slow phase velocities indicating close by, near-surface disturbances. Soft thresholding results also show occasional long period noise bursts which are a result of incomplete noise removal. These can be removed very easily by an extra step of band-pass thresholding but were included in the BBfk computation to gauge the effect of the noise in degrading the BBfk response. Obviously, the BBfk response is not significantly affected with the P wave showing up as a highly focused arrival at the correct backazimuth from the array (Figure 17).

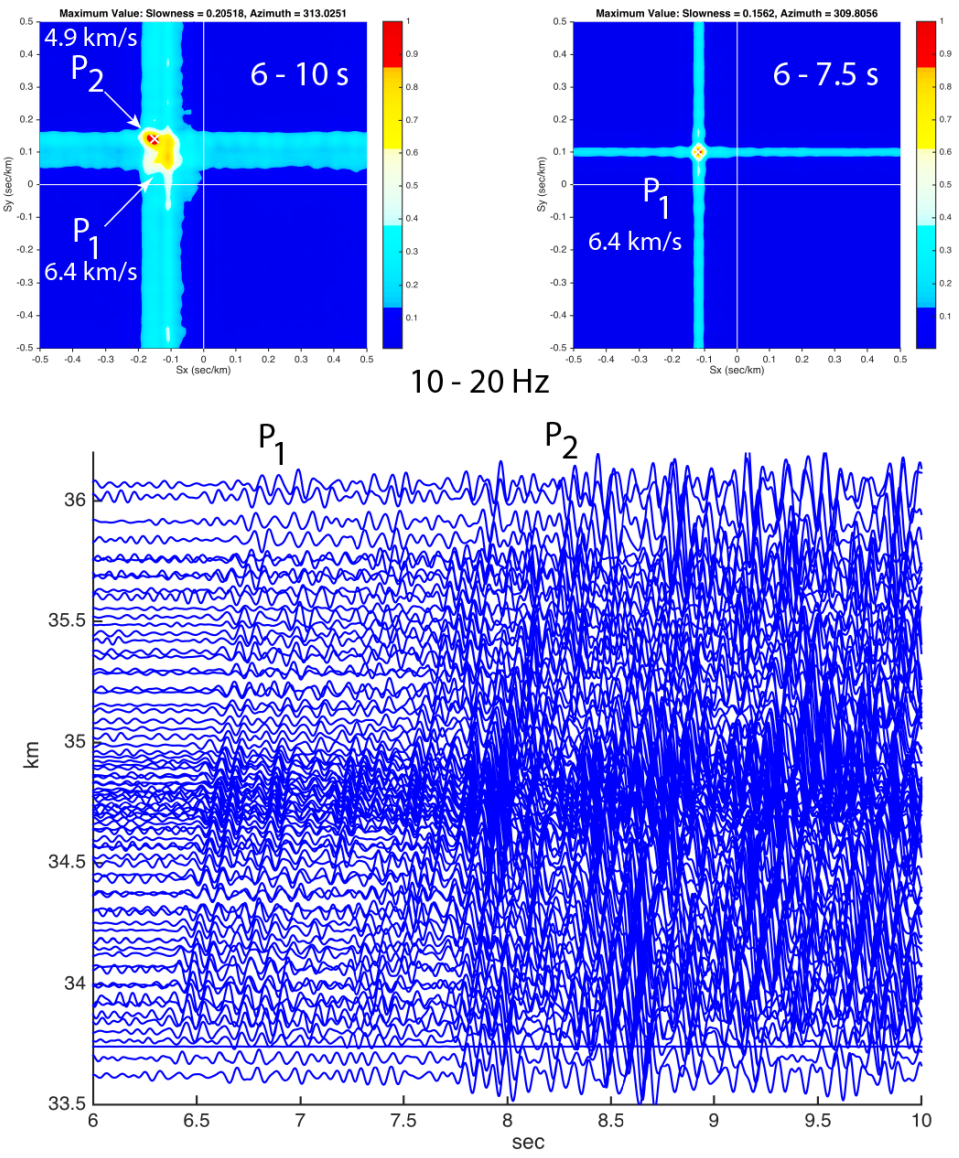

Figure 14 – Analysis of P wave phases from the 81-element Cross array. *The data (lower panel) have been filtered between 10 and 20 Hz and show at least 2 phases with differing phase velocities. The BBfk for the entire time window of 6 to 10 s (upper left) shows that P_2 dominates the response. Windowing only P_1 yields a high resolution estimate of its phase velocity and backazimuth (upper right).*

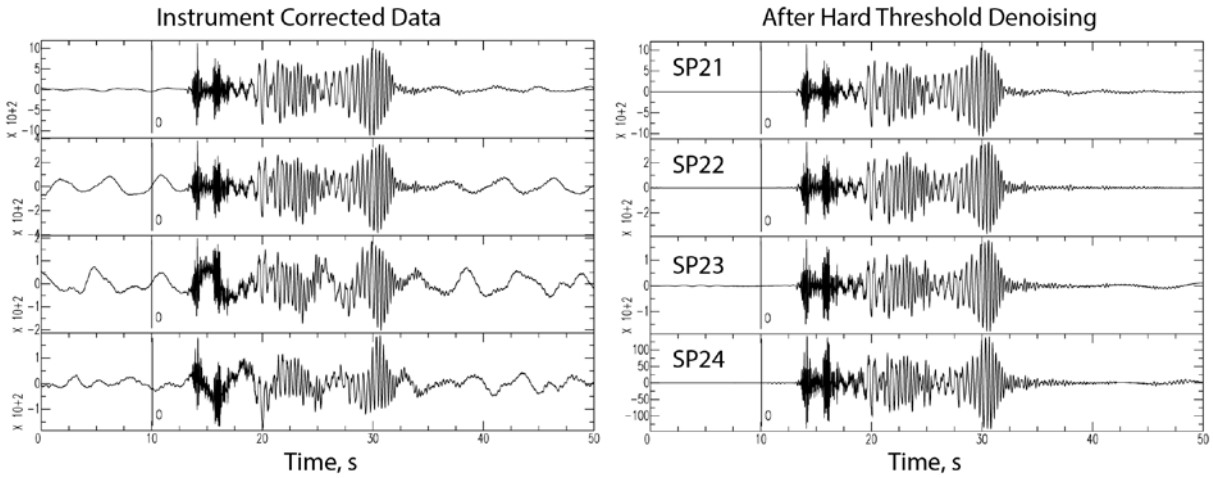

Figure 15 – Comparison of vertical component waveforms from nodal station 5014 in the IRIS experiment. *Instrument corrected data are shown in the left panel and denoised data shown in the right panel. The noise was estimated using 60s of ground motion before the P arrival and denoised using the hard threshold method. Note the high correlation between phases in the waveforms showing that CWT techniques did not produce much distortion in the waveform even though different noise levels were used in the denoising procedure.*

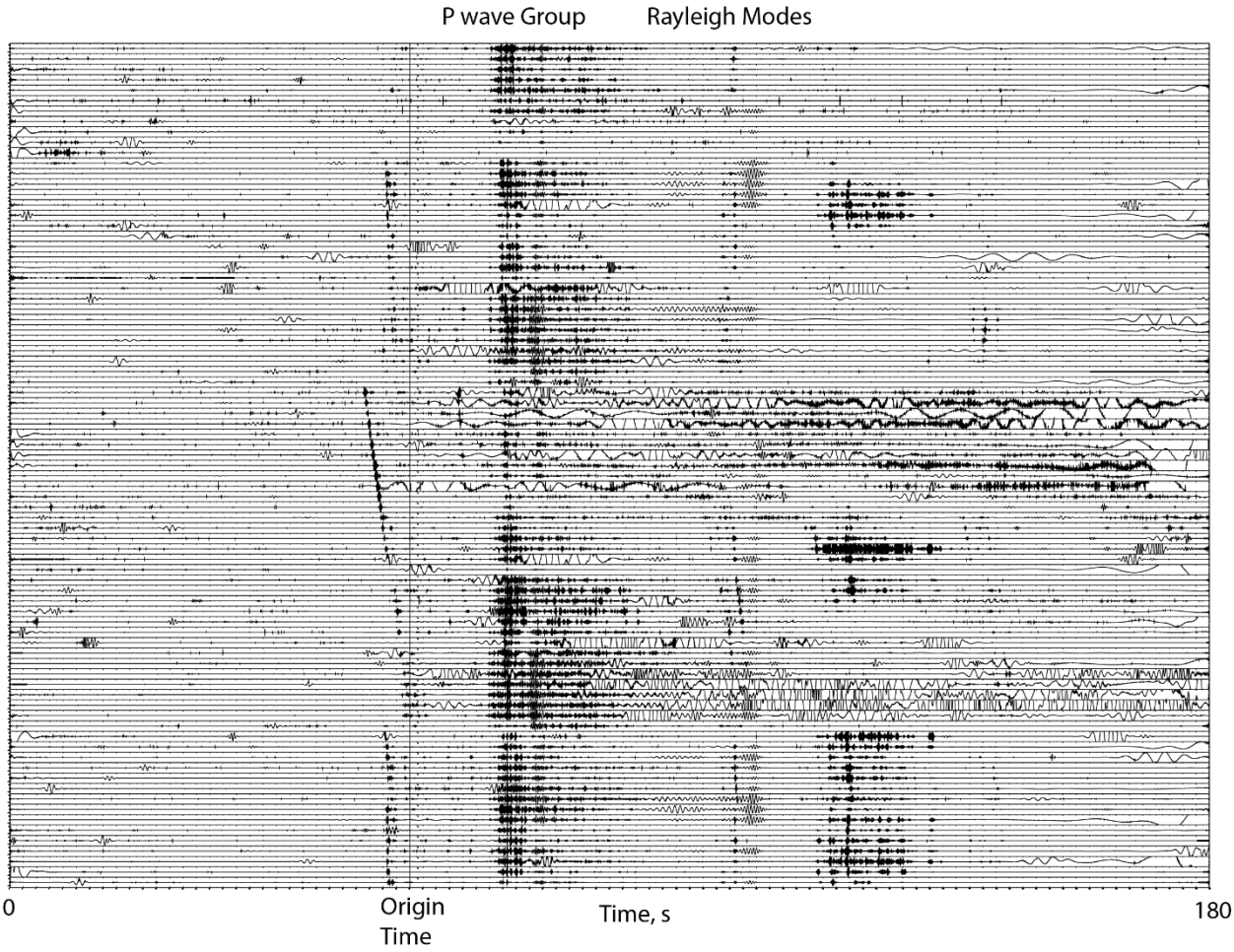

Figure 16 – Shotpoint 31 denoised data for the 81 elements of the eastern cross array. *The data were denoised using the soft thresholding technique. The P wave group is quite evident as well some of the Rg wavetrains. Note the numerous background seismic events at local distances showing up as diagonal streaks of high frequency arrivals across the array.*

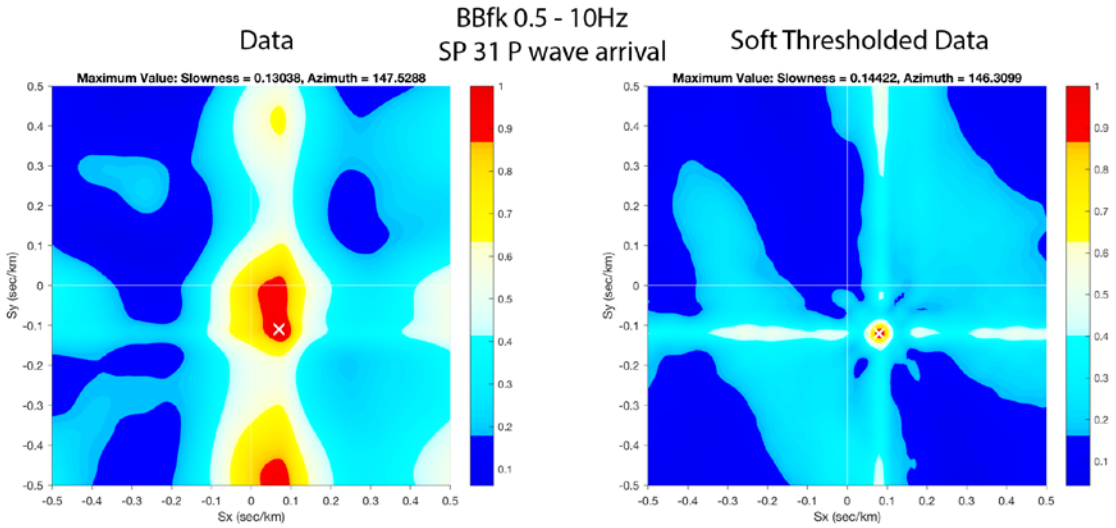

Figure 17 – BBfk responses of two seconds of record around the first P wave arrival. The left panel shows the slowness plot for the raw data. The right panel is for the denoised data of Figure 8. *The bandpass for the BBfk computation is relatively broad, 0.5 – 10Hz, and covers the dominant band of the nodal seismometers. The image is clearly focused using the denoised data. The BBfk of the raw data has large contributions of noise at large slowness from a power windfarm south of the array. This is an example of the use of CWT thresholding techniques in improving phased array-derived wave attributes.*

3.4.3. Application to Detection of a Suspected North Korean Nuclear Test

Zhang and Wen (2015) and Kim et al. (2016) presented studies of a possible North Korean low-yield nuclear test that is inferred to have occurred on 12 May 2010. The initial seismological search was motivated by observations of radionuclides that were detected in mid-May by the CTBTO monitoring system (De Geer, 2012 and other references reviewed in Zhang and Wen 2015). Zhang and Wen (2015) performed an extensive search involving correlation of template explosions with available data from the GSN and Chinese seismic networks to make a good case for a very small, mb(Lg)=1.44, low-yield (29t) explosion at the North Korean test site. Subsequently, Kim et al. (2016) used other Chinese network data in addition to data collected by the IRIS/PASSCAL experiment NECESS that cast some doubt on Zhang and Wen's interpretation by suggesting that the event in question was more "earthquake-like" from P/S wave ratios and that the relative location may place it further from the test site. The somewhat different interpretations notwithstanding, detection and study of such a small event is truly remarkable and is at the limits of seismological practice.

We obtained NECESS experiment data, used by Kim et al. (2016), from the IRIS data archives to investigate whether CWT thresholding methods could help detect the event (Figure 18). Hard thresholding was applied by using a noise estimate calculated from 200s of data before the origin time suggested by Zhang and Wen (2015). Hard thresholding clearly exposed the event at station NE3C along with numerous other local earthquakes

and possible anthropological sources. The noise reduction is dramatic. Figure 19 compares the hard-thresholded, three-component data with results from Kim et al. (2016) for the same station. Major P and S wave phases are clearly seen in the thresholded data.

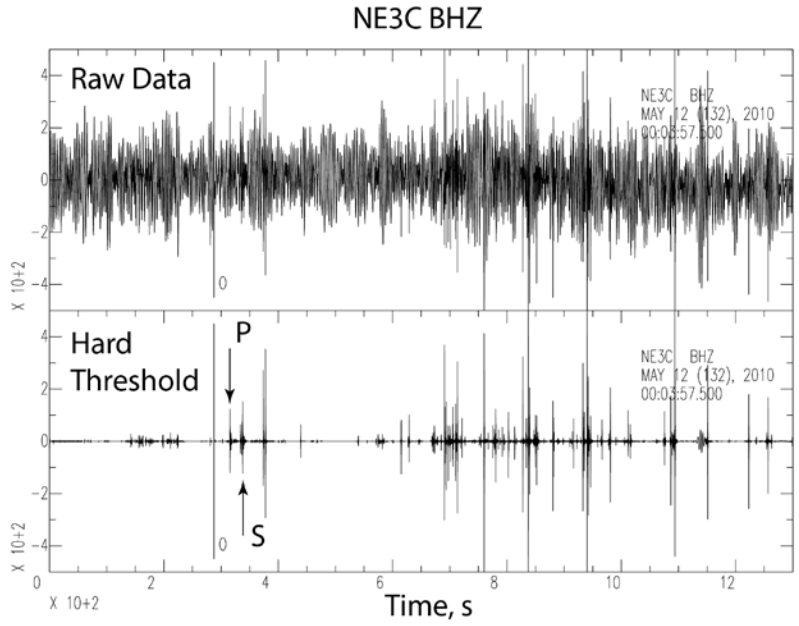

Figure 18 – Results of hard thresholding the raw velocity data from station NE3C of the NECESS PASSCAL experiment. *NECESS (Northeast China Extended Seismic Array) was deployed between September 2009 and August 2011. The raw data (upper panel) were thresholded to yield the seismogram in the lower panel by calculating a noise estimate from the seismogram 200s before the origin time (vertical line annotated with "O"). P and S wave arrivals for the mystery event are shown. Numerous other events are seen in the thresholded data.*

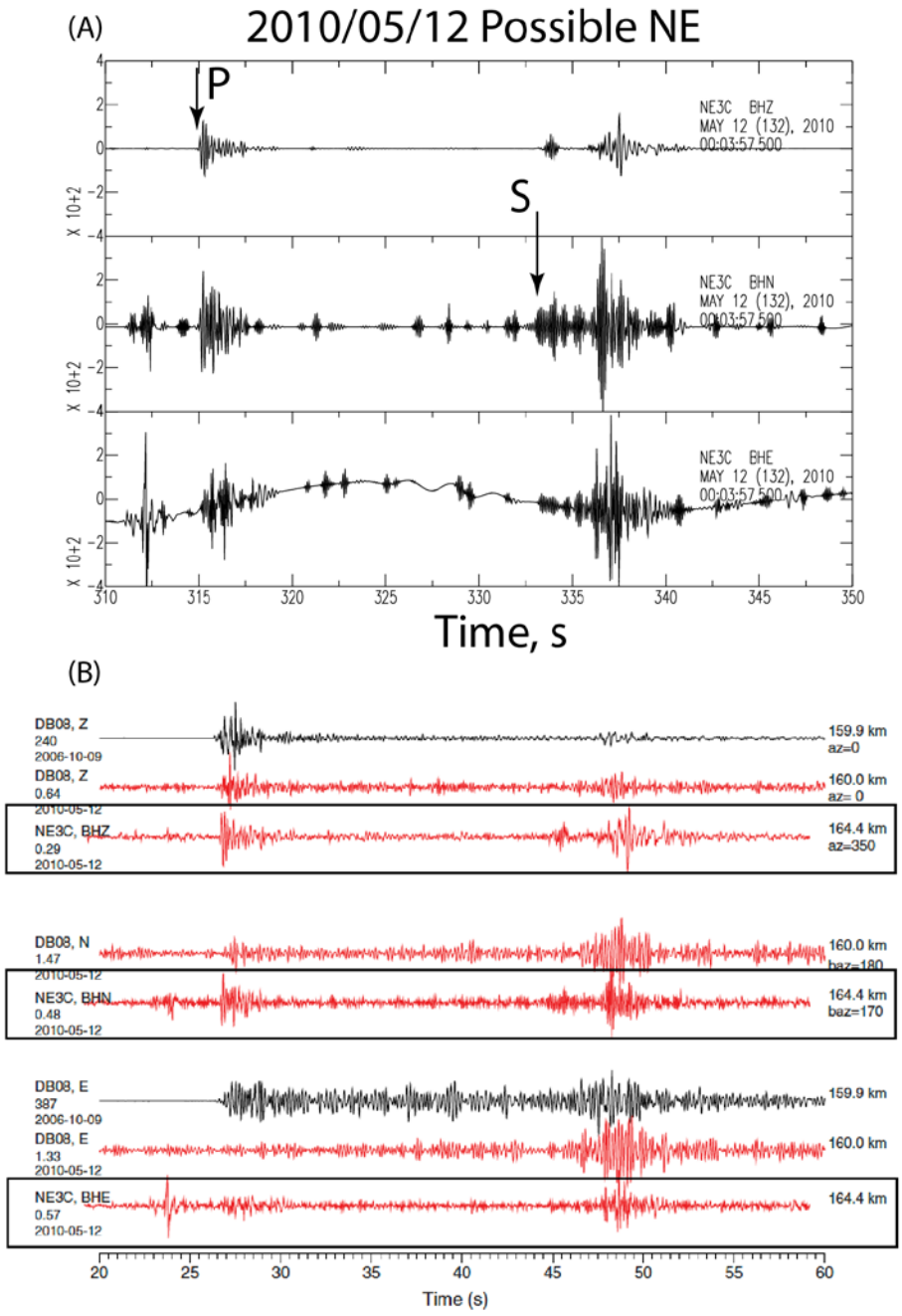

Figure 19 – Comparison of the hard-thresholded, three-component data at NE3C station (A) with bandpass filtered data presented in Figure 8 of Kim et al. (2016), (B). Inferred P and S wave arrivals for the small event are shown. *Boxes are drawn around the NECESS data displayed in Kim et al.'s figure.*

4. CONCLUSIONS

The use of TFR methods and transforms different from the Fourier transform in seismic data analysis has slowly grown over the past 20 years but it is surprising that these new methods have not caught on more quickly. Thresholding methods associated with the CWT offer a reasonably fast way to intuitively investigate noise and signal fields in seismograms. Relatively simple hard or soft thresholding methods have many attributes common with more computationally intense methods involving the SS-CWT and adaptive thresholding. The software tool developed in this contract, BCseis, allows an analyst to experiment with the data to gain an intuitive view of both signal and noise as well as understanding individual waves or wavetrains through interactive block thresholding.

Thresholding methods work for discrete seismic events because signals are often localized in areas of the TFR and can be separated from the noise through thresholding methods. The simple aphorism "signal occurs where noise is not" is the usual operative in the methods explored in this contract. As with other standard noise reduction methods, the case of overwhelming noise masking the signal over the TFR can cause these methods to fail. A fruitful, future research direction involves gathering such signals within the data with a separate processing step similar to template matching or match filtering before applying thresholding.

We found that dramatic signal-to-noise ratio improvement could be attained with simple hard or soft thresholding of the continuous wavelet transform. Single trace seismic data from explosions recorded at NVAR from the Source Physics Experiment, local explosions recorded by the IRIS Community Wavefields Experiment, and a suspected North Korean test could be simply and quickly converted into nearly noise-free seismograms with these techniques. Mixed results were obtained with a straightforward application of thresholding before beam forming at array sites. Thresholding made little difference in the analysis of SPE-3 data recorded at NVAR for the frequency band of 1-3 Hz. In fact, setting the threshold too high removed much of the lower frequency signal that correlated across the array yielding a poor result. Setting the threshold lower still produce good SNR improvement and allowed beamforming to give the correct answer. Thresholding the explosion data did help in focusing the beam pattern for explosion P waves recorded by a dense high-frequency array at the IRIS experiment. In any case, having a densely sampled, in space, high-frequency array was found to give superior results in analyzing seismic phases over sparsely deployed arrays such as NVAR or the Golay 3x6 broadband array at the IRIS experiment, thresholding techniques notwithstanding. A well-conceived data collection experiment is preferable over signal analysis techniques that require various assumptions. Nevertheless, the techniques explored here give an entirely different view of the seismic data that can be used to appreciate the nature of noise and signal. Perhaps the most revolutionary result of this research is the ability to dissect a seismogram into component wavetrains. It seems likely that interactive block thresholding will be very useful in studying seismic coda and the propagation of local/regional seismic phases.

References

Ahrabian, A. and D. P. Mandic, 2015, A Class of Multivariate Denoising Algorithms Based on Synchrosqueezing, IEEE Transactions on Signal Processing, **63**, pp. 2196-2208, doi:10.1109/TSP.2015.2404307.

Auger, F., P. Flandrin, Y. T. Lin, S. McLaughlin, S. Meignen, T. Oberlin, and H. T. Wu, 2013, Time-frequency reassignment and Synchrosqueezing: an overview, IEEE Signal Processing Magazine, **30**, pp. 32-41, doi:10.1109/MSP.2013.2265316.

Auger, F. and P. Flandrin, 1995, Improving the Readability of Time-Frequency and Time-Scale Representations by the Reassignment Method, IEEE Transactions on Signal Processing, **43,** pp. 1068-1089, doi:10.1109/78.382394.

Bekara, M. and M. van der Baan, 2009, Random and Coherent Noise Attenuation by Empirical Mode Decomposition, Geophysics, **74,** no. 5, pp. V89-V98, doi:10.1190/1.3157244.

Bonar, D. and M. Sacchi, 2012, Denoising seismic data using the nonlocal means algorithm, Geophysics, 77, pp. A5-A8.

Carmona, R. A., W. L. Hwang, and B. Torresani, 1997, Characterization of Signals by the Ridges of Their Wavelet Transforms, Signal Processing, IEEE Transactions, **45**, pp. 2586-2590.

Chassande-Mottin, E., I. Daubechies, F. Auger, and P. Flandrin, 1997, Differential Reassignment, IEEE Signal Processing Letters, **4** , pp. 293-294, doi:10.1109/97.633772.

Chen Y., J. Ma, and S. Fomel, 2016, Double-sparsity dictionary for seismic noise attenuation, Geophysics, **81**, no. 2, pp. V17-V30.

Chen, Y. and J. Ma, 2014, Random Noise Attenuation by F - X Empirical Mode Decomposition Predictive Filtering, Geophysics, **79**, no. 3, **pp.** V81–V91.

Daubechies, I., J. Lu, and H. Tieng Wu, 2011, Synchrosqueezed Wavelet Transforms: An Empirical Mode Decomposition-like Tool, Applied and Computational Harmonic Analysis, **30**, pp. 243-261, doi:10.1016/j.acha.2010.08.002.

Daubechies, I. and S. Maes, 1966, A Nonlinear Squeezing of the Continuous Wavelet Transform Based on Auditory Nerve Models, in Wavelets in Medicine and Biology, pp. 527-546, eds. A. Aldroubi and M. Unser, CRC Press.

De Geer, L.-E., 2012, Radionuclide evidence for low-yield nuclear testing in North Korea in April/May 2010, *Sci. Global Secur.*, 20, pp. 1-29.

Ditommaso, R., M. Mucciarelli, M. R. Gallipoli, and F. C. Ponzo, 2010, Effect of a single vibrating building on free-field ground motion: numerical and experimental evidences, Bull. Earthquake Eng. **8**, pp. 693-703, doi:10.1007/s10518-009-9134-5. Ditommaso, R., M. Mucciarelli, and F. C. Ponzo, 2012, Analysis of non-stationary structural systems by using a band-variable filter, Bull. Earthquake Eng, **10**, pp. 895-911, doi:10.1007/s10518-012-9338-y.

Douglas, A., 1997, Bandpass Filtering to Reduce Noise on Seismograms: Is There a Better Way? Bulletin of Seismological Society of America, **87,** pp. 770-777. Ford, S. R. and W. R. Walter, 2015, International Monitoring System correlation detection at the North Korean Nuclear Test Site at Punggye-ri with insights from the Source Physics Experiment, Seism. Res. Lett., **86**, no. 4, pp. 1160-1170, doi:10.1785/0220150029.

Galiana-Merino, J. J., J. Rosa-Herranz, J. Giner, S. Molina, and F. Botella, 2003, De-Noising of Short-Period Seismograms by Wavelet Packet Transform, Bulletin of Seismological Society of America, **93,** pp. 2554-2562, doi:10.1785/0120010133.

Gómez, J. L. and D.R. Velis, 2016, A simple method inspired by empirical mode decomposition for denoising seismic data, Geophysics, 81, no. 6, pp. V403-V413, doi:10.1190/GEO2015-0566.1.

Goupillaud, P., A. Grossmann, and J. Morlet, 1985, Cycle-octave and related transforms in seismic signal analysis, *Geoexploration*, 23, pp. 85-102.

Grossmann, A., R. Kronland-Martinet, and J. Morlet, 1989, Reading and understanding the continuous wavelet transform, in J. Combes, A. Grossmann, And P. Tchamitchian (eds.) *Wavelets: Time-Frequency Methods and Phase-Space*, 2-10, Springer, New York.

Han, J. and M. van der Baan, 2015, Microseismic and Seismic Denoising via Ensemble Empirical Mode Decomposition and Adaptive Thresholding, Geophysics, **80,** no. 6, pp. KS69-KS80, doi:10.1190/geo2014-0423.1.

Herrera, R. H., J. B. Tary, M. van der Baan, and D. W. Eaton, 2015, Body Wave Separation in the Time-Frequency Domain, IEEE Geoscience and Remote Sensing Letters, **12**, pp. 364-368, doi:10.1109/LGRS.2014.2342033.

Herrera, R. H., J. Han, and M. van der Baan, 2014, Applications of the Synchrosqueezing Transform in Seismic Time-Frequency Analysis, Geophysics, **79,** no. 3, pp. V55-V64, doi:10.1190/geo2013-0204.1.

Hou, T. and Z. Shi, 2013, Data-driven time–frequency analysis, Appl. Comput. Harmon. Anal., **35**, pp. 284-308

Huang, W., R. Wang, Y. Chen, H. Li, and S. Gan, 2016, Damped multichannel singular spectrum analysis for 3D random noise attenuation, Geophysics, **81**, no. 4, pp. V261-V270.

Huang, N. E., Z. Shen, S. R. Long, M. C. Wu, H. H. Shih, Q. Zheng, N.-C. Yen, C. C. Tung, and H. H. Liu, 1998, The Empirical Mode Decomposition and the Hilbert Spectrum for Nonlinear and Non-Stationary Time Series Analysis: Proceedings of the Royal Society A, Mathematical, Physical and Engineering Sciences, **454**, pp. 903-995, doi:10.1098/rspa.1998.0193.

Huang, Z. l., J. Zhang, T. H. Zhao, and Y. Sun, 2015, Synchrosqueezing S-Transform and Its Application in Seismic Spectral Decomposition, IEEE Transactions on Geoscience and Remote Sensing, **54**, pp. 817-825, doi:10.1109/TGRS.2015.2466660.

Iatsenko, D., P. V. E. McClintock, and A. Stefanovska, 2015, Linear and Synchrosqueezed Time-Frequency Representations Revisited: Overview, Standards of Use, Resolution, Reconstruction, Concentration, and Algorithms, Digital Signal Processing: A Review Journal, **42,** pp. 1-26, doi:10.1016h/j.dsp.2015.03.004.

Kim, W.-Y., P. G. Richards, D. P. Schaff, and K. Koch, 2016, Evaluation of a seismic event, 12 May 2010, in North Korea, Bull. Seism. Soc. Am., **107**, pp. 1-21, doi:10.1785/0120160111.

Li H., R. Wang, S. Cao, Y. Chen, and W. Huang, 2016, A method for low-frequency noise suppression based on mathematical morphology in microseismic monitoring, Geophysics, **81**, no. 3, pp. V159-V167.

Meignen, S., T. Oberlin, and S. McLaughlin, 2012, A New Algorithm for Synchrosqueezing, With an Application to Multicomponent Signals Sampling and Denoising: IEEE Transaction on Signal Processing, **60**, pp. 5787-5798.

Mousavi, S. M., C. A. Langston, and S. P. Horton, 2016a, Automatic Microseismic Denoising and Onset Detection Using the Synchrosqueezed-Continuous Wavelet Transform, Geophysics, **81**, no. 4, pp. 1-15, doi:10.1190/GEO2015-0598.1.

Mousavi, S. M. and C. A. Langston, 2016a, Hybrid Seismic Denoising Using Higher-Order Statistics and Improved Wavelet Block Thresholding, Bulletin of Seismological Society of America, 106, doi:10.1785/0120150345.

Mousavi, S. M. and C. A. Langston, 2016b, Adaptive noise estimation and suppression for improving microseismic event detection, Journal of Applied Geophysics, 132, pp. 116-124, http://dx.doi.org/10.1016/j.jappgeo.2016.06.008.

Mousavi, S. M. and C. A. Langston, 2016c, Fast and novel microseismic detection using time-frequency analysis, SEG Technical Program Expanded Abstracts, 2632-26, doi:10.1190/segam2016-13262278.

Mousavi, S. M. and C. A. Langston, 2017, Automatic noise-removal/signal-removal based on general-cross-validation thresholding in synchrosqueezed domains, and its application on earthquake data, Geophysics, **82**, pp. V211-V227, doi:10.1190/geo2016-0433.1.

Naghizadeh, M. and M. Sacchi, 2012, Multicomponent Seismic Random Noise Attenuation via Vector Autoregressive Operators, Geophysics, **77**, no. 2, pp. V91-V99, doi:10.1190/geo2011-0198.1.

Naghizadeh, M., 2011, Seismic Data Interpolation and Denoising in the Frequency-Wavenumber Domain, Geophysics, **77**, no. 2, pp. V71-V80. doi:10.1190/GEO2011-0172.1.

Nawab, S., F. Dowla, and R. Lacoss, 1985, Direction determination of wideband signals, IEEE Trans. Acous. Speech Sig. Proc., **33**, pp. 1114-1122.

Oropeza, V. and M. Sacchi, 2011, Simultaneous seismic data denoising and reconstruction via multichannel singular spectrum analysis: Geophysics, **76**, no. 3, pp. V25-V32.

Parolai S., 2009, Denoising of Seismograms Using the S Transform: Bulletin of Seismological Society of America, **99**, pp. 226-234, doi:10.1785/0120080001.

Pazos, A., M. J. Gonz, and G. Alguacil, 2003, Non-Linear Filter, Using the Wavelet Transform, Applied to Seismological Records: Journal of Seismology, **7**, pp. 413-429.

Pinnegar, C. R. and D. W. Eaton, 2003, Application of the S transform to prestack noise attenuation filtering: J. Geophys. Res. **108**, p. 2422, doi:10.1029/2002JB002258.

Sabbione, J. I., M. D. Sacchi, and D. R. Velis, 2013, Microseismic Data Denoising via an Apex-Shifted Hyperbolic Radon Transform, SEG Annual Meeting, 22-27 September, Houston, Texas.

Sabbione, J. I., M. D. Sacchi, and D. R. Velis, 2015, Radon transform-based microseismic event detection and signal-to-noise ratio enhancement, Journal of Applied Geophysics, **113**, pp. 51-63.

Scherbaum, F, 2001, Of Poles and Zeros: Fundamentals of Digital Seismology: January, Kluwer Academic Publishers, http://dl.acm.org/citation.cfm?id=517106.

Schimmel, M. and J. Gallart, 2007, Frequency-Dependent Phase Coherence for Noise Suppression in Seismic Array Data: Journal of Geophysical Research, Solid Earth, **112**, pp. 1-14, doi:10.1029/2006JB004680.

Shuchong, L. and C.n Xun, 2014, Seismic Signals Wavelet Packet de-Noising Method Based on Improved Threshold Function and Adaptive Threshold, Computer Modeling and New Technologies, **18**, pp. 1291-1296.

Sobolev, G. and A. Lyubushin, 2006, Microseismic impulses as earthquake precursors: Izvestiya, Physics of the Solid Earth, **42**, pp. 721-733, doi:10.1134/S1069351306090023.

Snelson, C. M., R. E. Abbott, S. T. Broome, R. J. Mellors, H. J. Patton, A. J. Sussman, M. J. Townsend, and W. R. Walter, 2013, Chemical explosion experiments to improve nuclear test monitoring, EOS, **94**, pp. 237-239.

Starck, J.-L., F. Murtagh, and J. M. Fadili, 2010, *Sparse Image and Signal Processing*, Cambridge University Press, New York, New York.

Thakur, G. and H. T. Wu, 2011, Synchrosqueezing-Based Recovery of Instantaneous Frequency from Nonuniform Samples, SIAM Journal on Mathematical Analysis, **43**, pp. 2078-2095, doi:10.1137/100798818.

Thakur, G., E. Brevdo, N. S. Fučkar, and H. T. Wu, 2013, The Synchrosqueezing Algorithm for Time-Varying Spectral Analysis: Robustness Properties and New Paleoclimate Applications, Signal Processing, **93**, pp. 1079-1094, doi:10.1016/j.sigpro.2012.11.029.

Tselentis, G. A., N. Martakis, P. Paraskevopoulos, A. Lois, and E. Sokos, 2012, Strategy for Automated Analysis of Passive Microseismic Data Based on S-Transform, Otsu's Thresholding, and Higher Order Statistics, Geophysics, **77**, no. 6, p. KS43, doi:10.1190/geo2011-0301.1.

Velis, D., J. I. Sabbione, and M. D. Sacchi, 2015. Fast and automatic microseismic phase-arrival detection and denoising by pattern recognition and reduced-rank filtering, Geophysics, **80**, no. 6, pp. WC25-WC38, doi:10.1190/GEO2014-0561.1.

Yang, H., 2015, Synchrosqueezed Wave Packet Transforms and Diffeomorphism Based Spectral Analysis for 1D General Mode Decompositions, Applied and Computational Harmonic Analysis, **39**, pp. 33-66, doi:10.1016/j.acha.2014.08.004.

Yang, H. and L. Ying, 2014, Synchrosqueezed Curvelet Transform for Two-Dimensional Mode Decomposition, The SIAM Journal on Mathematical Analysis, **46**, pp. 2052-2083.

Zhang, L., Y. Wang, Y. Zheng, and X. Chang, 2015, Deblending using a high-resolution radon transform in a common midpoint domain, J. Geophys. Eng., 12, pp. 167-174.

Zhang, M. and L. Wen, 2015, Seismological evidence for a low-yield nuclear test on 12 May 2010 in North Korea, Seism. Res. Lett., 86 (1), pp. 138-145, doi:10.1785/02201401170.

LIST OF SYMBOLS, ABBREVIATIONS AND ACRONYMS

AFRL	Air Force Research Laboratory
AFSPC	Air Force Space Command
AFTAC	Air Force Technical Applications Center
BT	Block Thresholding
CC	Correlation Coefficient
CWT	Continuous Wavelet Transform
EMD	Empirical Mode Decomposition
GCV	General Cross Validation Thresholding
HOS	Higher Order Statistics
IMF	Intrinsic Mode Function
NLM	Non Local Means
OBS	Ocean Bottom Seismometer
RMSE	Root-mean-square error
SNR	Signal to Noise Ratio
SS	Synchrosqueezing
SS-CWT	Synchrosqueezed Continuous Wavelet Transform
STFT	Short Time Fourier Transform
TFR	Time-Frequency Representation
WHT	Wavelet Hard Thresholding
WSC	Wavelet Squared Coherency
XWT	Cross Wavelet Spectrum

DISTRIBUTION LIST

DTIC/OCP
8725 John J. Kingman Rd, Suite 0944
Ft Belvoir, VA 22060-6218 1 cy

AFRL/RVIL
Kirtland AFB, NM 87117-5776 1 cy

Official Record Copy
AFRL/RVBYE/Dr. Frederick Schult 1 cy

This page is intentionally left blank.